Review Article

# Quantitative imaging techniques for the assessment of osteoporosis and sarcopenia

**Sara Guerri[1,2], Daniele Mercatelli[1], Maria Pilar Aparisi Gómez[3,4], Alessandro Napoli[5], Giuseppe Battista[2], Giuseppe Guglielmi[6,7], Alberto Bazzocchi[1]**

[1]The Unit of Diagnostic and Interventional Radiology, The "Rizzoli" Orthopaedic Institute, Bologna, Italy; [2]Department of Experimental, Diagnostic and Specialty Medicine, Division of Radiology, S.Orsola-Malpighi Hospital, University of Bologna, Bologna, Italy; [3]Department of Radiology, Auckland City Hospital, Grafton, Auckland, New Zealand; [4]Department of Radiology, Hospital Nueve de Octubre, Valencia, Spain; [5]Radiology Section, Department of Radiological, Oncological and Anatomopathological Sciences, "Sapienza" University of Rome, Rome, Italy; [6]Department of Radiology, University of Foggia, Foggia, Italy; [7]Department of Radiology, Scientific Institute "Casa Sollievo della Sofferenza" Hospital, San Giovanni Rotondo, Foggia, Italy

*Correspondence to:* Sara Guerri, MD. Department of Experimental, Diagnostic and Specialty Medicine, Division of Radiology, S.Orsola-Malpighi Hospital, University of Bologna, Via G. Massarenti 9, Bologna 40138, Italy. Email: guerri.sara@gmail.com.

**Abstract:** Bone and muscle are two deeply interconnected organs and a strong relationship between them exists in their development and maintenance. The peak of both bone and muscle mass is achieved in early adulthood, followed by a progressive decline after the age of 40. The increase in life expectancy in developed countries resulted in an increase of degenerative diseases affecting the musculoskeletal system. Osteoporosis and sarcopenia represent a major cause of morbidity and mortality in the elderly population and are associated with a significant increase in healthcare costs. Several imaging techniques are currently available for the non-invasive investigation of bone and muscle mass and quality. Conventional radiology, dual energy X-ray absorptiometry (DXA), computed tomography (CT), magnetic resonance imaging (MRI) and ultrasound often play a complementary role in the study of osteoporosis and sarcopenia, depicting different aspects of the same pathology. This paper presents the different imaging modalities currently used for the investigation of bone and muscle mass and quality in osteoporosis and sarcopenia with special emphasis on the clinical applications and limitations of each technique and with the intent to provide interesting insights into recent advances in the field of conventional imaging, novel high-resolution techniques and fracture risk.

**Keywords:** Osteoporosis; sarcopenia; absorptiometry; photon; multidetector computed tomography (CT); magnetic resonance imaging (MRI)

Submitted Nov 10, 2017. Accepted for publication Jan 17, 2018.
doi: 10.21037/qims.2018.01.05
**View this article at:** http://dx.doi.org/10.21037/qims.2018.01.05

## Introduction

Bone and muscle are two deeply interconnected organs with integrated functions in growth and locomotion (1). A strong relationship exists between their development, maintenance and correct functioning, from which the concept of "bone-muscle unit" derives (2). Muscle and bone interactions take place at different levels (organ, cellular, and molecular level) with bidirectional pathways. Mechanical loading and muscle contraction are the most important determinants of bone mass and shape, and physical activity (PA) is known to exert an anabolic effect on the metabolism of both these tissues (2-4). A linear relationship exists between bone mineral content (BMC) and lean body mass (2,5,6). The rise in life expectancy in developed countries resulted in the progressive increase in the prevalence of chronic degenerative diseases, with particular emphasis on those affecting the musculoskeletal system. Osteoporosis and

 

sarcopenia are two widespread diseases of increasing public interest and represent an important area of investigation of geriatric and nutritional research. Recently, a rapid increase in the knowledge of the pathologic processes associated with the aging of the musculoskeletal system, together with important advances in the field of high resolution imaging techniques, have improved dramatically our understanding of osteoporosis and sarcopenia.

Different imaging modalities are available for a non-invasive evaluation of bone and skeletal muscle mass and quality in osteoporosis and sarcopenia. Dual energy X-ray absorptiometry (DXA), computed tomography (CT), magnetic resonance imaging (MRI) and ultrasound are of variable importance in the study of osteoporosis and sarcopenia and often play a complementary role, depicting different aspects of the same pathology (7,8).

This paper aims to review the role of different imaging modalities currently available for the non-invasive investigation of bone and skeletal muscle in osteoporosis and sarcopenia, highlighting the main limitations of conventional imaging techniques, the potential value of recently developed diagnostic tools and novel advances in the field of high resolution imaging, which provide useful insights into pathophysiology and fracture risk.

## Clinical implications

Osteoporosis is defined as "a skeletal disorder characterized by compromised bone strength predisposing to an increased risk of fracture" (9). Bone strength, a term commonly used to describe the health of bone and its ability to resist fracture, is primarily affected by two parameters, namely, bone density and bone quality (10,11). Bone density expresses the amount of mineral per unit area or volume, while bone quality refers to the complex microarchitecture and peculiar composition of bone tissue (9). In 2010 osteoporosis affected about 27.6 million adults in Europe and 53.6 million adults in the United States were estimated to have osteoporosis or low bone mass at either the femoral neck or lumbar spine (12,13). Osteoporotic fractures represent a major cause of morbidity and mortality in elderly population and are associated with a significant increase in healthcare costs. In Europe the cost of osteoporosis (including cost of incident fractures, cost of long-term disability and cost of pharmacological fracture prevention) was estimated at approximately 37.4 billion euro in 2010 (12). In the United States the annual estimated cost associated with osteoporosis-related fractures amounted to 16.9 billion dollars in 2005 and it is expected to rise to 25.3 billion dollars in 2025 (14,15).

The term sarcopenia derives from the Greek term "sarx" or flesh + "penia" or loss and it was used for the first time in 1989 to describe the age-related loss of muscle mass (16). However, a broadly accepted definition of sarcopenia is not yet agreed upon. To address this gap, the European Working Group on Sarcopenia in Older People (EWGSOP, the Sarcopenia Working Group) was created in 2009. According to EWGSOP, sarcopenia is defined as a "syndrome characterized by progressive and generalized loss of skeletal muscle mass and strength", stressing the importance of the decrease of muscle function (i.e., muscle strength or performance) for the diagnosis (17). The estimated prevalence of sarcopenia varies extremely within different cohorts according to patients' characteristics, ranging from 0.1% to 85.4% in adult subjects (18). The prevalence of this condition differs also depending on the definition used for its diagnosis. According to the EWGSOP definition, the prevalence of sarcopenia is 1–29% for older adults living in the community and 14–33% in long-term care populations (19). Sarcopenia is associated with many adverse outcomes like increases in morbidity and mortality, hospitalization, physical disability and loss of independence in activities of daily living (20,21). Data concerning the health-care costs of sarcopenia are largely lacking. The very few studies available in this field reported that the direct cost of sarcopenia (estimated on the basis of the medical expenditures associated with physical disability in older persons and attributable to sarcopenia) in the United States was approximately of 18.5 billion dollars in 2000 (22). To the best of our knowledge, no similar study has been performed in Europe.

The development and the maintenance of bone mass and muscle mass are deeply related, and both are affected by age. The peak of both bone and muscle mass is achieved in early adulthood, followed by a progressive decline after the age of 40 (20,23). After the age of 50, the decline of muscle mass becomes more substantial proceeding at a rate of 1% per year (23,24). The decline in the total amount of bone and muscle mass is accompanied by concomitant modifications of their cells population (25). In bone tissue, the aging process is characterized by a progressive accumulation of adipose cells within the bone marrow (BM). The role of marrow adipose tissue (MAT) as an important component of the BM microenvironment has been deeply investigated in the last few years and a growing body of evidence shows an inverse association between MAT content and both bone

 

**Figure 1** "Picture frame" appearance of vertebral bodies on lateral lumbar spine view. As result of resorption processes, vertebral bodies show an overall increase in radiolucency and a thin and well-demarcated cortical rim.

mineral density (BMD) and bone integrity (25-29). Estrogen deficiency, prolonged glucocorticoid treatment, altered leptin signaling, disuse and bed-rest are some of the most important conditions known to be associated with BM adipogenesis and, according to recent evidences, they are also responsible for the fatty infiltration of skeletal muscles (myosteatosis) (25). Two different pathways are implicated in the development of myosteatosis: (I) the accumulation of intracellular lipids within the myofibers (intramyocellular lipids), which is associated with decreased insulin sensitivity and inflammation; and (II) the disproportioned differentiation to the "adipogenic lineage" of the mesenchymal stem cells population, which is responsible for the accumulation of inter-myofiber fat. Fatty infiltration in skeletal muscles is responsible for a decreased insulin sensitivity and has a detrimental effect on muscle health and function (25). The term "sarcopenic obesity" is currently used to describe the co-existence of loss of muscle mass and increased adiposity, resulting in a relative increase in fat mass (FM) compared to lean muscle mass, and it is currently recognized as an important aspect of frailty in older adults (20,25,30-32). The mean Hounsfield unit (HU) of the lean tissue within the mid-thigh muscle bundle, obtained by CT scan, was used by Lang *et al.* as an indicator of intramuscular fat infiltration. After adjustment for age, race, gender, height, body mass index (BMI), and total percentage of body fat (measured with DXA), a significant association was found between decreased thigh muscle attenuation and increased risk of hip fracture [relative risk/standard deviation (RR/SD) =1.58] and this association remained significant after further adjustment for total femur BMD (33). Muscle weakness is also the most important individual risk factor for falls in older people, being associated with an approximately 4.4-fold increase in mean attributed risk (34-36). This data is of particular clinical interest, considering that sarcopenia is a potentially treatable condition, if interventions are initiated early (37).

## Conventional radiography

Findings suggestive of osteoporosis are frequently encountered on radiographs and it is extremely important for the radiologist to be aware of them. The main radiographic features of osteoporosis are: (I) increased bone radiolucency; (II) cortical thinning; (III) changes in the trabecular pattern (38,39). Increased bone radiolucency (I) results from the progressive decline in BMC and the concomitant impoverishment of the trabecular microarchitecture, resembling the appearance of an over-exposed radiograph. However, this feature is detectable only in the advanced stages of the disease, when the amount of bone loss reaches at least 30% (39). Cortical thinning (II) results from the reabsorption of the periosteal, intracortical and endosteal layers. The resorption process is very active in the endosteum because of its rich blood supply, resulting in a gradual widening of BM space. In the vertebral bodies, this feature together with the concomitant increase in bone radiolucency is responsible for the typical "picture frame" appearance, also known as "ghost vertebra" (*Figure 1*) (38,39). In the early-stages of osteoporosis, a scalloping in the inner margin of the cortex, known as "endosteal scalloping", can be seen, but this finding is non-specific and can be found also in pathologic conditions characterized by rapid bone turn-over like hyperparathyroidism, renal osteodystrophy or reflex sympathetic dystrophy syndrome. Lastly, the alteration in trabecular pattern (III) is caused by the fact that trabeculae, which are more abundant in the axial skeleton and at the ends of long bones, offer a greater surface area for resorption processes and respond faster to metabolic changes than cortical bone (38,39). Early on, secondary trabeculae, which are not primarily involved in weight bearing, are lost first, while the primary trabeculae become more prominent and will disappear only at a later stage. Using these specific and predictable sequence of resorptive processes, some authors developed

 

semi-quantitative indexes for the diagnosis and grading of osteoporosis. Among these indexes, those proposed by Singh *et al.* considering the proximal femur and by Jhamaria *at al.* considering the calcaneus were perhaps the most widely used ones in the past (40-42). However, these indexes suffer from a great inter-observer variation and the quality of the radiographs itself and the superimposition of soft tissues (with particular regards to the Singh index) can also affect the results. An extended description of these indexes is beyond the purpose of this article, and for a more comprehensive discussion, the interested reader is referred to the referenced publications (38,40-42).

Currently DXA represents the most widely used technique for the assessment of BMD, thanks to its wide availability, the extremely low radiation dose and low costs. However, in the past, great efforts were undertaken to develop quantitative evaluation methods of osteoporosis from conventional radiography. Among these, radiographic absorptiometry (RA) and metacarpal radiogrammetry represent the oldest techniques (43).

The development of the principles behind RA first enabled BMD estimation (44). In this method, a radiograph of a peripheral site, typically metacarpals and phalanges, is obtained placing a reference wedge of hydroxyapatite or aluminum close to the bone. BMD is then expressed relative to the density of this wedge material (45). Even if RA was limited to peripheral skeletal sites, the composite volume density and the composite area density derived by RA at the phalanges showed a good correlation with the standard measurements of BMD derived by DXA (r=0.69 and 0.68 respectively, at lumbar spine; r=0.63 and 0.67 respectively, at the femoral neck) (45). However, RA was time consuming and results were strongly influenced by multiple factors including operator expertise, X-ray beam intensity and soft tissue thickness (43).

Radiogrammetry was introduced in 1960 and represents a simple and inexpensive method to evaluate cortical bone changes in tubular bones using plain radiographs. Radiogrammetry can be used in different bone segments. However, the second metacarpal of the non-dominant hand is the most common site of application (43). The metacarpal index (MCI), also known as Barnett-Nordin index, is expressed as the ratio between the combined cortical thickness (Ct.Th) (radial and the ulnar cortex) of the mid second metacarpal and the diameter itself of the shaft at this level, measured with a caliper (46,47). As medullary width and bone width (BW) both increase with aging due, respectively, to endosteal reabsorption and periosteal apposition, the MCI was used for a long time to obtain an objective evaluation of the degree of cortical bone loss in osteoporosis (43). The manual measurement technique represented the main limitation of radiogrammetry, with a high precision error (PE) and a great inter-observer variation (46). Recently, technological advances brought this old technique back into focus: in digital X-ray radiogrammetry (DXR) a computer automatically identifies the average Ct.Th and BW of the second, third and fourth metacarpal midshafts. The fully automated measurements obtained from three metacarpal bones, instead of one, are responsible for the enhanced accuracy and precision of DXR. From Ct.Th and BW measurements, a compound measurement called "bone volume per projected area" (VPA) is determined and BMD is then derived through a geometrical operation (43,48). In 1999 DXR was approved by the Food and Drug Administration (FDA) as a reliable method for estimating BMD. A significant correlation was proved to exist between DXR-derived BMD (DXR-BMD) at the three mid-metacarpals and DXA-derived BMD at the spine, total hip and distal radius (r=0.52, 0.55 and 0.76, respectively; P<0.0001 for all) (46). When five regions of interest (ROIs) were used to derive DXR-BMD (second, third, fourth mid-metacarpals and the distal radius and ulna) the level of correlation with DXA-derived BMD was even higher (r=0.86 at the distal forearm; r=0.79 at the ultradistal forearm; r=0.62 at the spine; r=0.69 at the total hip; r=0.73 at femoral neck; P<0.0001 for all) (48).

## DXA

The role of DXA is central in the study of body composition (BC) thanks to its ability to differentiate FM, non-bone lean mass (LM) and BMC at both the regional and the whole-body level (*Figure 2*) (49-60). DXA relies on the use of two X-ray beams of different energy; the measurement of the "R value" is calculated as the ratio between the degree of attenuation of the lower energy and the higher energy beam. The R value is specific for each tissue and depends on the patient's soft tissue composition. From the R value, using complex algorithms, it is possible to derive the amount of BMC in pixels containing bone. BMD is then calculated as the ratio BMC/area (in g/cm$^2$). In pixels without bone, soft tissue is further characterized as FM and non-bone LM (61,62).

### *DXA in osteoporosis*

Currently, DXA represents the gold standard for diagnosis

 

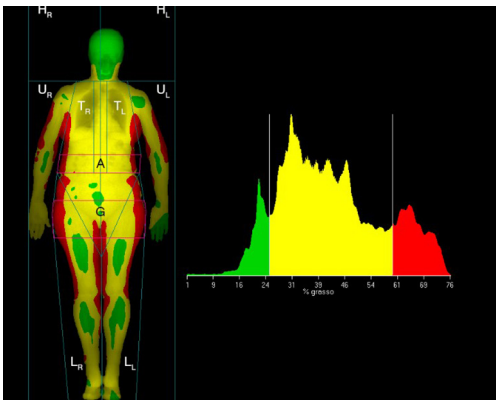

**Figure 2** Whole body DXA scan. The image on the left shows the standard ROIs used for regional body composition analysis: head (H), trunk (T), upper limbs (U), lower limbs (L), android (A) and gynoid (G) regions. The colored soft tissues map and the histograms (on the right) show the distribution of fat in different body segments (red areas: fat percentage >60%; yellow areas: fat percentage 25–60%; green areas: fat percentage <25%). DXA, dual energy X-ray absorptiometry; ROIs, regions of interest.

and monitoring of osteoporosis and low bone mass conditions (63). Several guidelines have been developed in recent years to ensure proper use of this densitometric technique, from appropriate indications for BMD testing to procedures for correct data analysis and reporting. In 2016, a panel of experts reviewed the current guidelines on DXA for adults: the overall quality of DXA guidelines was satisfactory and "Adult and Pediatric Official Positions" issued by the International Society for Clinical Densitometry (ISCD) achieved the highest total score according to the Appraisal of Guidelines for Research & Evaluation version II (AGREE II) (64). BMD is expressed in terms of SD comparing individual BMD measurement to a reference range derived from a population of healthy young adults (at peak bone mass) in the case of T-score, and from an age-matched population of the same gender and ethnic group in the case of Z-score. In post-menopausal women and in men older than 50 years old osteoporosis is defined as a T score of –2.5 or less at the lumbar spine (from L1 to L4), femoral neck or total hip. In pre-menopausal women and in men younger than 50 years old a Z-score of –2 or less is defined as "below the expected range for age" (63,65). In clinical practice, DXA generally represents the first exam performed in patients with suspected osteoporosis, thanks to its wide availability, low cost, and minimal radiation exposure [the effective dose to an adult from a spine and hip examination is approximately between 1 and 10 μSievert (μSv)] (66-68). Nonetheless, BMD measured by DXA accounts only for 60–70% of variation in bone strength and the majority of osteoporotic fractures occur in people whose BMD is in the non-osteoporotic range (69-71). This fact takes on particular importance in diabetes-related bone disease. Patients with diabetes mellitus (DM) show an increased risk of fractures, especially at the hip (summary RR for hip fractures according to two large meta-analyses: 6.3–6.9 in type 1 DM; 1.4–1.7 in type 2 DM) (72,73) that does not appear to be explained by the variation of BMD, which is just slightly reduced in type 1 DM and normal or even increased in type 2 DM in comparison with non-diabetic controls (29,74). In patients with type 2 DM, Janghorbani *et al.* documented a slightly elevated fracture risk at the ankle (RR =1.3), proximal humerus (RR =1.3), foot (RR =1.3; association statistically significant) and spine (RR =1.2) whereas de Liefde *et al.* documented an elevated overall risk of non-vertebral fractures (VFs) (hazard ratio: 1.69) despite the higher BMD values at the femoral neck and lumbar spine (72,75). These results show that BMD by itself underestimates fracture risk in diabetic patients. This evidence suggests that other additional factors like the deterioration of bone microarchitecture and the modification of BM microenvironment must be taken in consideration for the investigation of bone status (29,76).

Today, other parameters beyond BMD can be derived from DXA for a better understanding of bone strength. Trabecular bone score (TBS) is a novel gray-scale textural analysis recently approved by the United States FDA that can be derived from a previously acquired lumbar spine DXA scan, providing information about bone microstructure and bone strength. The major advantages of TBS are its simplicity and low cost, since TBS is measured in the same ROIs of the lumbar spine BMD (77-79). Dedicated software is used to measure the gray level of variation among pixels within the 2D DXA image and differentiate between bone structures with similar areal BMD (a-BMD) but different bone microarchitecture (*Figure 3*) (80). TBS is not a direct measure of trabecular microarchitecture, but it has been proved to be associated with vertebral, hip and major osteoporotic fracture risk in postmenopausal women and with hip and major osteoporotic fracture risk in men over 50 years of age (81). Specifically, each SD decline in TBS corresponds to a 20–50% increase in the risk of vertebral, hip and major osteoporotic fractures in postmenopausal women and to a 30–40% increase in risk of hip and major osteoporotic

 

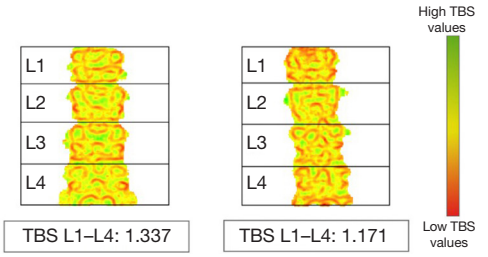


**Figure 3** TBS printouts in a healthy control, on the left (BMD L1–L4 =0.929 g/cm$^2$) *vs.* osteoporotic bone, on the right (BMD L1–L4 =0.799 g/cm$^2$). Local TBS values are displayed on previously acquired DXA scan using a color scale: areas colored in green indicate a good microarchitecture, areas colored in red indicate a deteriorated microarchitecture. TBS, trabecular bone score; BMD, bone mineral density; DXA, dual energy X-ray absorptiometry.

fractures in men over 50 years of age. However, according to ISCD guidelines, TBS should not be used alone in clinical practice but rather in combination with BMD and FRAX to enhance fracture prediction (81). For postmenopausal women the following range has been proposed: TBS >1.350, normal; TBS between 1.200 and 1.350, partially degraded microarchitecture; TBS <1.200 degraded microarchitecture; a similar range for men has not yet been proposed (79). TBS has also been proven to be associated with major osteoporotic fracture risk in postmenopausal women with type 2 DM, thus it may serve as an additional tool for fracture risk assessment in this selected class of patients (81-83). TBS can also be assessed in other conditions characterized by bone loss (as primary hyper-parathyroidism, rheumatoid arthritis, chronic kidney disease, etc.). However, further studies are needed to establish its use in these disorders (84,85).

Other non-BMD parameters can be derived from 2D DXA images in addition to TBS. Hip Structural Analysis (HSA; Hologic, Bedford, MA, USA) and Advanced Hip Assessment (AHA; GE-Lunar, Madison, WI, USA) are two recently developed software products that can be applied to a standard DXA scan to automatically derive various parameters related to bone geometry and bone strength, including hip axis length (HAL), cross sectional area (CSA), outer diameter (OD), section modulus (SM), buckling ratio (BR), cross-sectional moment of inertia (CSMI) and neck shaft angle (NSA) (86,87). According to the ISCD 2015 official positions, among hip geometry parameters derived from DXA, only the HAL is associated with hip fracture risk in postmenopausal women (88). HAL, by definition, is the distance (in mm) from the lower base of the greater trochanter, through the femur neck, to the inner pelvic brim (*Figure 4*). At the beginning of the 90s, Faulkner *et al.* demonstrated the existence of an association in postmenopausal women between a longer HAL and increased risk of femoral neck fractures (OR =1.9) and trochanteric fractures (OR =1.6) even after adjustment for age, femoral neck density, height, and weight. No significant association between the neck width or the NSA and risk of hip fracture was documented (89). Recently, Leslie *et al.* confirmed the role of HAL as a BMD and FRAX-independent risk factor for hip fracture in women and, additionally, reported the same independent effect of longer HAL on hip fracture risk in men (90,91). This data was however derived from a single clinical registry. These preliminary results, albeit promising, need further validation with large scale studies and at the current state of investigations, there is not sufficient evidence to support this statement in men.

### *DXA in sarcopenia*

CT and MRI are considered the gold standard for the assessment of skeletal muscle mass; however, the significant complexity and the high cost strongly limit their use (7). DXA is an attractive opportunity in the study of muscle mass both at whole body and regional level and, according to the EWGSOP, it represents the preferred alternative method in research setting and clinical practice (17,54,55). Previous studies reported a good level of correlation between the measurements of skeletal muscle mass at lower limbs derived by DXA and those derived by CT and MRI, even if DXA tends to underestimate the extent of sarcopenia in comparison with the latter two techniques (92,93). DXA specific measures of LM include lean mass index (LMI: total LM/height$^2$), appendicular lean mass (ALM: arms LM + legs LM) and appendicular lean mass index (ALMI: ALM/height$^2$) (94). ALMI is of high clinical significance, since the maintenance of appendicular skeletal muscle mass is critical in the preservation of mobility and functional independence in advanced age (95). According to ISCD guidelines, "low lean mass" could be defined using ALMI with Z-scores derived from a young adult, race, and sex-matched population, however the threshold for the definition of low LM is yet to be validated (96). In recent years, age- and sex-specific data on ALM derived from general population have

 

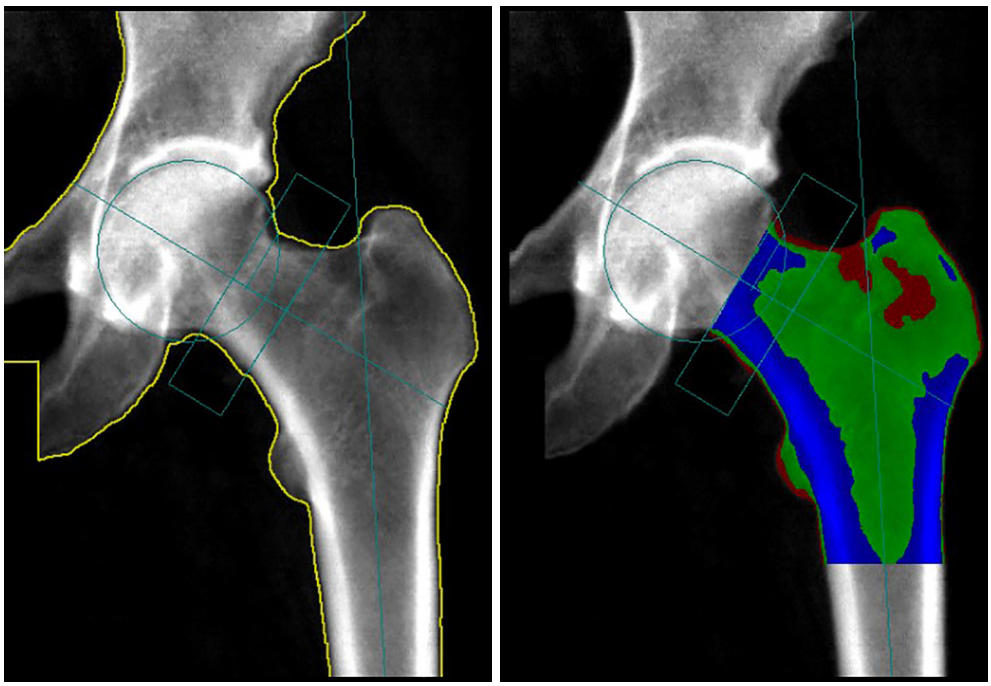

**Figure 4** Hip scan with hip geometry analysis. HAL is automatically traced throughout femoral neck from the lower base of the greater trochanter to the inner pelvic brim. The colored map on the right shows the different distribution of BMD values in different femoral regions (from blue to red—from high to low). HAL, hip axis length; BMD, bone mineral density.

been collected in different countries and could be useful in the future as a reference standard to monitor the wasting of muscle mass (97-101).

## CT

In daily practice, CT represents the most widely used 3D imaging modality. In the last few years, CT technology has evolved quickly and new advanced quantitative imaging modalities are available to study bone and muscle structures, in addition to the "standard" CT scan. Quantitative CT (QCT) and peripheral quantitative CT (pQCT) were originally designed to assess bone parameters respectively at central and peripheral sites, but are currently also used for the quantification of muscle mass and fat distribution (7,38). In the field of high-resolution imaging, high-resolution peripheral quantitative CT (HR-pQCT) represents an exceptional tool for 3D *in vivo* investigation of bone and muscle at peripheral sites (102).

### *CT in osteoporosis*

The usefulness of QCT in the study of osteoporosis is related to its ability to measure BMD in a chosen volume [volumetric-BMD (v-BMD)] without overlapping of other tissues and to the possibility of addressing cortical and trabecular bone separately (103,104). Compared to other imaging modalities, QCT has several advantages. QCT-derived v-BMD represents a true density measure expressed in g/cm$^3$, instead of an areal density as measured by DXA and may avoid the overestimation of BMD by DXA resulting from spinal degenerative changes, vascular calcifications and other sclerotic lesions in the surrounding soft tissues (105). QCT, compared to densitometric techniques, provides a measure of purely trabecular bone, which is more metabolically active and primarily affected by metabolic bone diseases, showing a better sensitivity for detecting osteoporosis than projectional methods (such as DXA) (103,106). For these reasons, QCT-derived T-scores cannot be used according to the WHO diagnostic classification since they are not equivalent to those obtained from DXA (105). QCT is generally applied to lumbar spine. Other measurement sites commonly evaluated include the proximal femur, forearm and tibia (105,107). In clinical application, spine and proximal femur are analyzed using standard whole-body CT scanners equipped with a

 

dedicated software for the analysis. According to the ISCD official positions with single-slice QCT, L1–L3 should be scanned, whereas with 3D QCT, L1–L2 should be scanned to limit the radiation dose (104,105). In QCT acquisition of the proximal femur the scan region should extend from the femoral head to the proximal shaft (108). Dedicated pQCT scanners (peripheral scanners, smaller and less expensive that whole body CT scanners) are used to evaluate v-BMD and bone microarchitecture at the distal radius and tibia: the 4% and 66% of the length of the radius and the 4%, 38%, 50% and 66% of the length of the tibia are the peripheral sites most commonly evaluated. Using pQCT, v-BMD can be derived and trabecular and cortical bone parameters can be assessed separately, allowing the examination of architectural and geometrical parameters such as Ct.Th, marrow and cortical CSA, both periosteal and endosteal circumference, as well as biomechanical parameters like CSMI (104,109).

In the last few years a large number of studies have evaluated the clinical utility of QCT in fracture prediction and longitudinal monitoring: according to the ISCD 2015 official positions, the ability of spinal trabecular BMD derived by QCT to predict spinal fractures in postmenopausal women is comparable to or better than that of lumbar spine BMD derived by DXA; sufficient evidence to support this statement in men is lacking (105). Total femur trabecular BMD derived by QCT has the capability to predict hip fractures as well as hip BMD derived by DXA in both menopausal woman and older men (110). QCT has also been extensively tested in monitoring age, disease and treatment related BMD changes (105,110). Despite this, for therapeutic decisions the role of DXA at the lumbar spine and femur remains central and in clinical practice DXA should be preferred to QCT to limit radiation exposure, unless QCT can provide superior information (110). Even QCT subjects the patients to a higher radiation exposure than DXA (radiation dose expressed as effective dose equivalent estimated for female QCT protocols: <1 mSv for single-slice QCT spine L1–L3; ~1.5 mSv for 3D QCT spine L1–L2; ~2.5–3.0 mSv for 3D proximal femur QCT; <0.01 mSv for pQCT forearm on clinical CT scanners) (105). Finally, the feasibility of opportunistic screening deserves a special mention. The term opportunistic denotes the use a pre-existing diagnostic CT scan (of the abdomen and pelvis) for the assessment of BMD to screen for patients at increased risk of fracture, without need for any additional DXA scan. In this context, the major disadvantages in comparison with QCT are the absence of an in-scan calibration phantom and the lack of a strictly standardized acquisition protocol. According to the ISCD 2015 official positions, the identification of patients with high fracture risk (according to low BMD or strength measures derived by CT at the spine or proximal femur) is possible with "standard" CT scan only if machine-specific cutoff values and scanner stability have been established (108).

Recently, dedicated high resolution pQCT scanners have been developed to evaluate bone microarchitecture in detail (104). HR-pQCT represents an attractive non-invasive technique to further investigate bone structure *in vivo*. Thanks to the high spatial resolution and the high signal-to-noise ratio (SNR) HR-pQCT can directly visualize trabecular microarchitecture at peripheral sites (normal isotropic voxel of 82 and 41 µm, respectively in older and newer scanner; trabecular dimension ~82 µm). HR-pQCT can assess BMD, microstructural and mechanical parameters of both cortical and trabecular bone separately at the distal radius and tibia with a very low effective dose (~4.2 µSv) and without the involvement of radiosensitive organs (102,111). Even though HR-pQCT is limited to the appendicular skeleton, a good correlation has been proven between density (a-BMD and v-BMD), geometry (CSA) and stiffness parameters measured peripherally and those derived by QCT at lumbar spine and proximal femur, the sites where the vast majority of osteoporotic fractures occur (112,113). HR-pQCT specific measures of BMD include whole bone v-BMD and, after the segmentation of the cortical and trabecular compartments, trabecular bone BMD (Tb.BMD) and cortical bone BMD (Ct.BMD); a-BMD of the ultradistal radius can be accurately estimated from 3D-HRpQCT image data with results that strongly correlate with DXA measurements (114,115). In addition, different microstructural bone parameters can be assessed, including bone volume ratio (BV/TV, %), average trabecular number (Tb.N, 1/mm), average trabecular thickness (Tb.Th, mm), average trabeculae separation/spacing (Tb.Sp, mm) and individual trabecula segmentation (ITS) (114). In particular, ITS refers to trabecular orientation and the ratio of rod-like and plate-like trabeculae, which have been recognized as important determinants of bone strength (116). Recently, the use of HR-pQCT has allowed interesting insights into the investigation of bone deterioration in secondary osteoporosis and related bone diseases (114). Using HR-pQCT at the distal radius and tibia, Stein *et al.* documented that postmenopausal women with primary hyperparathyroidism (PHPT) have thinner cortices, reduced Tb.BMD and Ct.BMD in comparison with healthy controls; in the PHPT group, ITS analyses documented a large heterogeneity in the

 

distribution of the trabeculae and a depletion of plate-like trabeculae, with a lower trabecular plate-to-rod ratio (117). In postmenopausal women with type 2 DM and history of fragility fractures HR-pQCT documented that both cortical bone porosity and pore volume are increased at the distal radius and distal tibia (significantly greater intra-cortical pore volume, relative porosity and endocortical bone surface at the ultra-distal and distal tibia; 4.7-fold greater cortical porosity at the distal radius; higher intra-cortical pore volume and larger trabecular heterogeneity at the ultra-distal radius) (118). The increased cortical porosity and the impaired trabecular microarchitecture among type 2 DM patients could explain, at least in part, the high incidence of fragility fractures, despite the normal or even elevated a-BMD derived from DXA examination (119).

### *CT in sarcopenia*

Together with MRI, CT represents the gold standard for investigating BC and to assess quantitative and qualitative changes in muscle mass. Measuring the attenuation of an X-ray beam crossing different tissues, a CT scan can differentiate between fat and fat-free mass. Zero and 100 HU are respectively the upper and lower threshold values commonly used to identify skeletal muscle tissue; a reduced muscle attenuation reflects an increased amount of fat within muscle (120). Normal density muscles show attenuation values in the range of 31–100 HU (within 2 SD of the mean attenuation value observed in lean normal muscle) while low-density muscles show attenuation values in the range of 0–30 HU (121). Quantification of skeletal muscle composition and adipose tissue distribution from different body segments and individual muscle groups can be achieved with a high level of accuracy using dedicated mathematical reconstruction algorithms. Mitsiopoulos *et al.* reported an excellent level of correlation between CT-derived CSA ($cm^2$) values of arm and leg adipose tissue-free skeletal muscle (ATFSM), adipose tissue surrounding muscle and adipose tissue embed within muscle (interstitial adipose tissue) and those obtained from cadaveric studies (r=0.97, 0.99 and 0.96, respectively); similarly good results were observed between cadaveric and CT volume estimates for the same three compartments (122). The use of CT to assess skeletal muscle mass is however limited in clinical practice by the high radiation dose, high cost and operational complexity (7). Although it was originally designed to assess bone structure, pQCT can also be used for soft tissue area quantification, being increasingly used to investigate the complex relationships between bone, muscle and fat. Traditionally, pQCT analysis was limited to the peripheral limbs (generally at 66% of the length of the tibia, the area with the largest muscle CSA within the lower leg, and at the mid-forearm), however newer scanners with larger gantries also allow the study of the mid-thigh. As whole-body CT, pQCT can provide CSA of soft tissue and estimate muscle density, while having the important advantages of an extremely low effective dose and relatively low cost (7). Since with pQCT fat is calibrated to zero, typical muscle density ranges from 65 to 90 $mg/cm^3$ (120). In individuals with a great amount of fat within and between myofibers, density values are lower. Muscle CSA and muscle density can be derived with dedicated manufacturer software after the delineation of the muscle-subcutaneous fat boundary in a semi-automated manner, even if these boundaries may not be immediately apparent (requiring a greater manual intervention to delineate muscle from surrounding fat) (123). An important limitation of pQCT is the lack of homogeneity in the protocols for image acquisition and analysis: the large majority of the studies published in this field examined muscle mass at the 66% tibia and 65% radius sites, but this is not an absolute rule (other studies evaluated for example the 38% or 55% sites) (7).

## MRI

Unlike CT which uses ionizing radiation to produce diagnostic images, MRI is based on the absorption and emission of radiofrequency energy by hydrogen nuclei (contained in large abundance in water and fat) under the influence of an applied external magnetic field. In the study of BC, variations in radiofrequency pulse sequence are used to differentiate between adipose tissue and fat-free mass: adipose tissue is characterized by a short T1 and a long T2 proton relaxation time (124). The lack of ionizing radiation is one of the major advantages of MRI, making it particularly suitable for long-term follow-up and for monitoring disease progression and treatment efficacy. The opportunity to study the trabecular network extended the use of MRI for the investigation of the mechanisms of age/disease-related bone weakening (38). T1- and T2-weighted imaging, chemical shift imaging, diffusion weighted imaging (DWI), dynamic contrast enhanced perfusion MRI and proton magnetic resonance spectroscopy (H-MRS) are just some of the MRI-imaging based approaches to investigate

 

BC and bone status.

### *MRI in osteoporosis*

Recent advances in MRI technology have brought significant progress to the study of osteoporotic bone, allowing the assessment of the features of trabecular bone and hence of its biomechanical proprieties (125). The investigation of trabecular network with MRI is however, perhaps, less intuitive than with QCT and HR-pQCT because the physical principles underlying the generation of diagnostic images are complex and completely different from those of X-ray based techniques (126). In MRI, cortical bone appears dark (or as a signal void) due to the very small number of mobile protons and the extremely short T2 relaxation time; the trabecular bone network also appears as a signal void but the surrounding BM gives rise to a high signal, which intensity depends on the amount of fatty content (*vs.* hematopoietic BM) (102,127). Differences in diamagnetic susceptibility at the interfaces between BM and trabecular bone structure cause a reduction of marrow relaxation time T2*, and the extent of this decay depends on density and microarchitecture of the surrounding trabeculae (126) Today, high resolution MRI allows the depiction of trabecular bone density and structure *in vitro* and *in vivo* with a high spatial resolution (in-plane resolutions as high as 78 µm; slice thickness of approximately 300 µm) (8,102,128,129). If at the beginning, the study of trabecular microarchitecture and cortical bone was limited to peripheral sites (like the radius, tibia and calcaneus), the use of optimized pulse sequences, high magnetic field systems (3 Tesla) and phased array coils led to enhanced SNR, allowing the investigation of deep-seated skeletal sites, such as the proximal femur (130). The potential of MRI as a diagnostic modality for the assessment of trabecular bone without the use of ionizing radiation has to be considered, however some limitations must be taken into account. At resolutions similar to individual trabeculae dimension, partial volume effects may arise; additionally, MRI is time consuming and technically challenging and the MRI protocol best suited for the study of trabecular bone is still being debated (131). Since QCT and HR-pQCT can directly depict the trabecular network, in our opinion, they represent the most suitable techniques for the investigation of trabecular bone; however, comparing high-resolution MRI with QCT and HR-pQCT, recent studies have documented that MRI performs equally well with trabecular bone measurements (129,131,132). Three classes of structural parameters can be derived from MRI, namely, scale, topology and orientation. Scale refers to structural parameters analogous to standard histomorphometry, including apparent BV/TV, apparent Tb.Th, apparent Tb.Sp and apparent Tb.N; topology refers to the structure of the trabeculae themselves that can be "rod-like" or "plate-like"; finally, orientation refers to the degree of anisotropy of the structure (102). Analyzing femoral head specimens, Sell *et al.* found a high degree of correlation between trabecular bone structure measures obtained by 3T MRI and by micro-CT (µCT), as the standard of reference ($r^2$ for App. BV/TV =0.82; $r^2$ for App. Tb.Sp =0.84; $r^2$ for App. Tb.N =0.81; $r^2$ for App. Tb.Th =0.67) (133). MRI-derived measures of trabecular architecture were shown to be distinctively affected by osteoporosis (e.g., high Tb.Sp; low BV/TV, Tb.Th and Tb.N), and may be used, in combination with DXA measures, for an improved prediction of osteoporotic fractures (134-136). Wehrli *et al.* demonstrated that the conversion of trabecular structure in the distal radius from "plate-like" to "rod-like" and the disruption of rodlike trabecular elements were significantly associated with the extent of vertebral deformities, determined by a semi-automated approach on sagittal MRI sequences (137). MRI also has the ability to depict cortical bone three-dimensionally: among cortical parameters that can be investigated, cortical porosity and Ct.Th are of particular clinical importance, as stressed above (102). Recently, ultra high-field (7 Tesla) MRI has shown its potential in the field of research thanks to the high SNR and increased spatial resolution, that allows a more accurate depiction of trabecular bone microarchitecture (138). Using 7 Tesla MRI equipment, Guenoun *et al.* demonstrated a significant association between bone microarchitecture parameters from cadaveric lumbar spine specimens (e.g., BV/TV; Tb.Th and Tb.Sp measured in axial and sagittal planes) and biomechanical parameters (failure load and the failure stress determined with biomechanical compression test) (139).

Today MAT is consensually recognized as an important component of the BM microenvironment; in particular a negative association exists between MAT content and BMD and bone integrity (140). H-MRS is an interesting extension of diagnostic MRI that can be used not only to quantify MAT content but also to further investigate its composition (141,142). H-MRS-based analysis of MAT composition is an emerging field of research in diabetic patients,

 

who generally show a lower unsaturated lipid fraction in comparison with healthy controls (29).

### *MRI in sarcopenia*

MRI represents the most advanced and most fascinating technique in the study of BC and skeletal muscle. MRI allows not only the quantification of muscle size (CSA, volume), but also the comprehensive assessment of muscle quality (143,144). Similarly to CT, Mitsiopoulos *et al.* reported an excellent level of correlation between MRI-derived CSA ($cm^2$) values of ATFSM, adipose tissue surrounding muscle and adipose tissue embed within muscle (interstitial adipose tissue), and those obtained from cadaveric studies (r=0.97, 0.99 and 0.92, respectively); similarly good results were observed between cadaveric and MRI volume estimates for the same three compartments (122). A key advantage of MRI, in comparison with other imaging techniques, is the capability to detect changes in the muscle structure occurring with aging and disease progression. In this regard, abnormal edema and the progressive accumulation of adipose tissue and fibrous connective tissue (both non-contractile tissues) within muscles contribute to loss of muscle strength and quality, which has increasingly been recognized as a critical aspect of aging and sarcopenia (143,144). Two-point Dixon-based technique and chemical shift-based water-fat separation are two quantitative MRI techniques that have been frequently applied to objectively measure muscle fat content (145-147). Finally, the amount of intramyocellular lipid, which is negatively correlated to insulin sensitivity, can be quantified by H-MRS (143,148-150). Over the last few years, many studies have focused on age-related changes in skeletal muscle mass. In a large cohort of healthy adults (men: n=268; women: n=200) Janssen *et al.* observed that the loss of skeletal muscle mass with advancing age was more relevant in the lower limbs in comparison with the upper limbs for both men and women (151). Using MRI, several studies documented substantial differences in the composition of muscular groups of the lower limbs in the elderly in comparison with young people. Kent-Braun *et al.* documented a larger contractile CSA of the tibialis anterior muscle in healthy young subjects (25–45 years old) in comparison with older (65–85 years old) adults; in addition, the amount of non-contractile tissue (expressed as absolute and relative non-contractile areas) was smaller in the first group (152). Similarly, Macaluso *et al.* documented a significantly lower amount of muscle contractile volume and a significantly greater amount of intramuscular non-contractile tissue in older women (mean age: 69.5±2.4 years) in comparison with young women (mean age: 22.8±5.7 years), in both quadriceps and hamstrings (153). In the study by Nilwik *et al.*, quadriceps muscle CSA was 14% smaller in the elderly group compared with young men and this difference was largely explained by a reduction in type II muscle fiber size (29%; P<0.001), with a concomitant tendency for smaller type I muscle fibers (P=0.052) (154).

All these features make MRI (together with CT) the gold standard in investigating muscle mass and quality in a research setting, however high cost, limited access to the equipment and its complexity limit the use of MRI in routine clinical practice (17,50). The lack of a standardized assessment protocol in image analysis represents a strong methodological weakness, limiting comparison between the results of different studies; in particular, tissue segmentation algorithms can vary a lot ranging from a manual segmentation technique to a fully automated method (7).

## Ultrasound

Thanks to its low cost, portability and the lack of ionizing radiation, ultrasound has gained increasing importance in clinical practice and currently represents an important tool to investigate osteoporosis and sarcopenia (155,156).

### *Quantitative ultrasound (QUS)*

QUS represents an effective alternative method for non-invasive evaluation of bone status; this technique analyzes the interactions between ultrasounds (frequency range employed between 200 kHz and 1.5 MHz) and bone tissue and provides insight complementary to that provided by densitometric techniques (157). Whereas bone density methods measure the X-ray attenuation in a given volume of tissue, QUS is based on the interaction and the propagation of ultrasounds (i.e., mechanical waves) across cortical and trabecular bone; QUS parameters reflect the structural anisotropy of bone, allowing to deduce its mechanical proprieties (156). The low cost, the portability and the lack of ionizing radiation represent the major advantages of QUS. Unfortunately, reproducibility of the results is a major concern and comparing measurements is difficult and sometimes misleading (156). The commercially available devices show great technological diversity (larger than what is commonly found in DXA) and employ different methods for calibration. For these reasons, according to the ISCD official positions, results from different devices cannot be

 

directly compared (158).

QUS specific measures of bone status include speed of sound (SoS), a parameter closely related to bone mineralization, and broadband ultrasound attenuation (BUA), which is closely related to structural characteristics of trabecular bone (104,157). A strong level of correlation has been found between heel trabecular transmission parameters (SoS and BUA) and BMD derived by DXA at lumbar spine and femoral neck (159,160). Other more complex parameters can be derived from the combination of SoS and BUA, such as amplitude dependent speed of sound (AD-SoS), stiffness and quantitative ultrasound index (QUI) (157,161). QUS is generally applied to peripheral skeletal sites, including the distal metaphysis of the phalanx, calcaneus, radius and tibia; however, the only validated measurement site in osteoporosis management is the heel. Validated heel QUS devices have been proved to predict fragility fractures in postmenopausal women (hip, vertebral, and global fracture risk) and in men over 65 years of age (hip and all non-VFs), independently of central DXA BMD (158).

QUS for the study of osteoporosis is completely validated and supported by scientific evidence. According to ISCD official positions, even though DXA remains the method of choice in clinical practice for therapeutic decisions, if a DXA scan cannot be performed, pharmacologic treatment can be initiated on the basis of a sufficient high fracture probability, assessed by heel QUS (using device specific thresholds) in conjunction with clinical risk factors (158). In particular, age over 75 years, BMI <20 kg/m$^2$, history of previous fractures after the age of fifty or falls within the last 12 months, maternal history of hip fracture, current smoking, DM, previous/current glucocorticoid treatment and use of arms to stand up from a chair are the clinical risk factors to take in account for decision making (158,162,163).

### *Skeletal muscle ultrasound*

Even if CT and MRI represent the gold standard in the study of BC, their use in daily clinical practice is not always feasible; ultrasound represents a convenient non-invasive technique to evaluate BC and muscle tissue (164). Its main advantages include simplicity, low cost and real time visualization of the target structure, without radiation exposure (165). Even though this technology is promising in geriatric practice, the technique of assessment is not completely standardized and, at the current state of knowledge, none of the operative definitions of sarcopenia includes ultrasound in its diagnostic algorithm (155). Ultrasound-derived measurements of muscle mass have shown a good-to-high level of correlation with those derived from reference methods (155,166-169). In 2005, Sanada *et al.* developed regression-based prediction equations for estimating total and regional skeletal muscle mass in healthy Japanese adults using ultrasound-derived muscle thickness taken at nine sites (lateral forearm, anterior and posterior upper arm, abdomen, subscapula, anterior and posterior thigh, anterior and posterior lower leg); a significant and strong site-matched correlation was found with MRI measured muscle mass (r=0.83–0.96 in men, r=0.53–0.91 in women, P<0.05) (170). Muscle thickness, CSA, echo intensity, fascicle length and pennation angle of the lower limbs (as sarcopenia preferentially affects postural muscles of the lower limbs such as the quadriceps femoris and gastrocnemius medialis) are the parameters most commonly evaluated by ultrasound examination; in pennate muscles, the pennation angle (defined as the angle formed at the attachment site of the fibers into deep and superficial aponeurosis) can be evaluated in static and dynamic conditions and provides information about mechanical and contractile proprieties (171). All of these parameters are affected by aging to a different extent but need to be further validated before their inclusion in diagnostic algorithms (155). The large majority of the available studies were conducted with small samples of healthy patients and no validated site-specific cut-off points for the ultrasound-based assessment of low muscle mass in geriatric patients exist. Minetto *et al.* were the first to collect and report muscle specific cut-off values for the detection of low muscle mass in the elderly (enrolled from institution-dwelling subjects with ≥1 of Fried's frailty criteria) (172).

## Quality assurance (QA) procedures

QA is defined as "a programme for the systematic monitoring and assessment of the various aspects of a service or facility to ensure that standards of quality are being met" (173). A QA program consists of five different parts: (I) guidelines and requirements for the correct installation of the facilities and their clinical use; (II) standardized periodic instrument quality control (QC) and technologists' QC; (III) preventive assessment of the condition of devices; (IV) training and education of technicians and radiologists performing and reporting the examination; (V) radiation safety policies and procedures (173,174). These aspects are of clinical importance in the management of osteoporotic patients and in the study of BC. QA procedures have been developed for

 

DXA, QCT, pQCT, HR-pQCT, MRI and QUS to ensure that accuracy and precision of the devices are consistent with manufacture guidelines (174,175). Accuracy is by definition the ability of a measurement to match the actual value of the quantity being measured and it is expressed in terms of accuracy error; precision, expressed in terms of PE, refers to the degree of reproducibility of repeated measurements under unchanged conditions (176).

To determine the accuracy of a DXA densitometer, a scan of a phantom of known density (density range and size of normal human spine) should be performed as often as possible (optimally three times a week, in any case, no less than once a week) to assess system calibration; phantom scanning and calibration should be repeated after any service is performed on the densitometer (65,173,174). PE of a DXA examination derives from the summation of inherent machine fluctuations and inaccuracies of the technologists performing the examination; the least significant change (LSC) enables the identification of statistically significant changes in BMD over time and is essential to make sure that any change observed in BMD measurement is real and not due to machine or to operator variability (176); the LSC can be calculated from PE using the ISCD precision calculating tool. Since the PE supplied by the manufacturer is not representative in general of the PE in the clinical setting, the ISCD recommends that each DXA center should determine its PE and LSC *in vivo*; if two or more technologists work on the same DXA scan, an average PE should be determined, combining data from all technologists (65). According to the ISCD, the minimum acceptable PE for an individual technologist [expressed as coefficient of variations (CV%)], is 1.9% at the lumbar spine, 1.8% at the total hip and 2.5% at the femoral neck; if the PE of a technologist exceeds these thresholds, retraining is required. In order to compare quantitatively to prior machine results, a cross calibration of DXA systems is required when (I) the DXA hardware has been changed, (II) when replacing a system with the same technology and (III) when changing the entire system to one made by the same manufacturer or different manufacturer (65).

One important advantage of BMD estimation by digital DXR is the high precision, which makes the technique particularly feasible for longitudinal studies. The short-term DXR precision has been shown to be superior to those of DXA at the hip and spine in both pre- and post-menopausal women and in both normal and osteoporotic subjects (46,48,177,178); in particular for DXR-BMD derived directly from digital hand radiographs (direct DXR), *in vitro* precision (expressed as CV%) ranged from 0.14% to 0.30%, while the *in vivo* precision for mean values of both hands was 0.46% (179). This means that DXR has the ability to detect any significant change in BMD in a very short period of time (thus to identify the progression of the disease or the response to treatment) and this supports the role of DXR-BMD as an important clinical tool for assessment of disease activity in rheumatoid arthritis (43,179).

ISCD recommendations are also available for DXA total BC with regional analysis; in this case the QC program should include adherence to manufacturer guidelines for system maintenance and, if not recommended in the manufacturer protocol, a BC phantom scan should be performed at least once a week to assess system calibration. Each technologist should perform an *in-vivo* precision assessment using patient's representative of the clinic's patient population; the minimum acceptable PE for an individual technologist is 3% for total FM, 2% for total LM and 2% for percent FM. *In-vivo* cross-calibration and cross calibration with a whole-body phantom are necessary to compare *in-vivo* results across different manufacturers and systems of the same make and model, respectively (65).

According to the ISCD official positions the following general recommendations should be followed for QCT, pQCT and QUS: (I) bone density measurements from different devices should not be directly compared; (II) device specific training and education of technicians and radiologists performing and reporting the examination should be provided; (III) QC procedures should be performed regularly (65).

QA of QCT systems represents as a main topic of investigation and recommendations for equipment specifications, equipment QC tests and radiation safety have been developed (174,180). PE depends on many factors including scanner model, scanning method, operator's skill, patient's positioning, ROI's positioning and collaboration of the patient during the examination; for these reasons, each QCT-center should perform a precision test to determine its PE and calculate LSC (174). In particular, the main source of error in determination of both Ct.BMD and Tb.BMD is represented by the partial volume effect. The presence of MAT results in an underestimation of bone density; the effect of marrow fat is more relevant at the spine and at the hip than at peripheral sites and is responsible for an accuracy error in the range of 5–15%, depending on age bands. This problem can be solved using age-related reference databases or, when available, using dual-energy QCT that recently gained popularity thanks

 

to the possibility to explore age, disease and drug-related effects on MAT (180). Finally, precision is enhanced with the use of 3D multidetector QCT in comparison with single slice 2D QCT technique, which is highly operator dependent (180).

Movement artifacts represent a significant source of error also in HR-pQCT examinations: although these errors can be minimized providing detailed instructions to the patients and by forearm or lower leg fixation, they can't be completely removed. The reproducibility of repeated measurements is generally affected by errors in repositioning (181). Recently, MacNeil *et al.* performed cadaveric forearm scanning, with and without repositioning, to determine the inherent reproducibility of the HR-pQCT technique (standard evaluation protocol based on the 2D area matching method); in the best scenario (without repositioning) the reproducibility measured in percent root mean squared (RMS) coefficient of variance was found to be less than 0.3%, while the reproducibility with repositioning error was less than 1.5%. The *in vivo* reproducibility of density, morphological and stiffness measurements was found to be less than 1%, 4.5% and 3.5%, respectively. When the standard evaluation protocol was repeated on the 3D registered data, repositioning error was reduced on average by 23% and 8% at distal radius and tibia, respectively (181). Similarly to QCT, daily and weekly QC programs should be conducted to identify drift, which can result as a consequence of decreased X-ray emission (109).

The reliability of pQCT for the analysis of muscle mass has been well established. For DXA, the ISCD recommends to assess the PE using the RMS approach from an assessment with 30 degrees of freedom to ensure the calculated PE is statistically accurate and unbiased, in order to identify the LSC (182). The same procedure should be used to assess the PE for pQCT (183). In the study by Swinford *et al.*, the overall relative PE calculated by the RMS method for pQCT measures (absolute and relative muscle and fat CSA, and muscle density) at 66% of tibial length was <1.5% and 3.0%, respectively for muscle and fat (184).

In ultrasound examinations, PE results from different factors, including incorrect positioning of the patient, coupling between the transducer and the skin and the effect of soft tissue properties (174). A constant check of the correct functioning of the probes and calibration of ultrasound signal emitted are mandatory to ensure the reliability of the technique (157,185). Each device has a specific calibration procedure and requires its own calibration phantom (generally composed of plastic material or Plexiglas) for QC (157). The ambient temperature itself can play a major role, influencing the coupling between probes and measurements sites. This is of particular importance in calcaneus devices that use water as coupling medium (186,187). In addition, the cross calibration of different devices represents an important concern in multicenter clinical studies and, even if many QUS models are currently available, their scientific validity was confirmed only in a small minority of cases (157). For all these reasons, the ISCD recommends not to use QUS to monitor the skeletal effects of treatments for osteoporosis (65). As stressed above, in the assessment of skeletal muscle mass and quality the lack of standardized protocols in image acquisition and image analysis and the operator dependence of ultrasound measures strongly limit the comparison of the results from different studies. Strasser *et al.* documented that ultrasound-derived measurements of muscle thickness assessed separately at the four heads of the quadriceps muscle in both young and elderly subjects were highly reproducible (intraclass correlation coefficients: 85–97%); on the contrary the reproducibility of echogenicity measurements differs between young (intraclass correlation coefficients: 57–65%) and old patients (intraclass correlation coefficients: 20–31%) (188).

MRI is affected by multiple technical and image quality problems and, even if several organizations suggested their QA recommendations and each manufacturer usually uses its own test protocols, the development of universally accepted guidelines would be desirable in MRI (175,189-191). To ensure high quality in radiology practice, the American College of Radiology (ACR) has proposed an accreditation program (i.e., a survey instrument to determine if standards are met) for MRI. The ACR method provides a comprehensive and easy to perform assessment of the performance of an MRI scanner and proved to be feasible in QA procedures (175,192). Its main advantages include the definition of a standardized image quality measurement protocol and the use of a standardized phantom developed specifically for the ACR to assess the technical quality of MRI sequences. The following technical parameters are evaluated for the assessments of MR image quality: high-contrast resolution, slice-thickness accuracy, geometric accuracy, slice position accuracy, signal uniformity, percent signal ghosting and low-contrast delectability (193).

## VFs assessment

As discussed, above the increased fracture risk represents the main clinical outcome of osteoporosis. In particular,

 


**Figure 5** VFA on lateral DXA scan. The placement of six vertebral points to determine vertebral heights is automated and the operator only needs to check for their correct positioning. VFA, vertebral fracture assessment; DXA, dual energy X-ray absorptiometry.

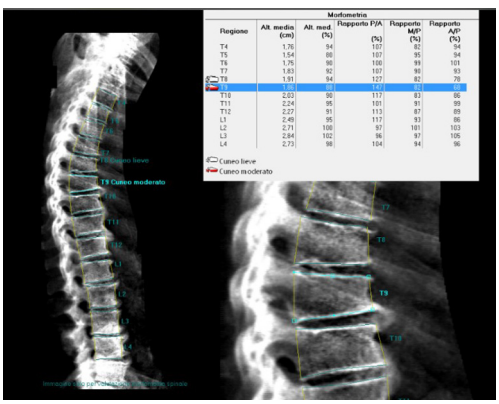


**Figure 6** Morphometric analysis of DXA spine image with accompanying chart (on the top right). The magnified view (on the bottom right) illustrates moderate wedging of the T9 vertebral body. DXA, dual energy X-ray absorptiometry.

VFs represent the hallmark of osteoporosis, accounting with a prevalence of about 35% to 50% among women over 50 years of age (194). VFs frequently occur in absence of a major trauma and are often asymptomatic (195,196). Despite this, the occurrence of a VF is very important in the management of osteoporotic patients since it results in an increase in the risk of experiencing a new incident VF and other fragility fractures. Women with a pre-existing VF suffer a 4- to 5-fold increase risk of sustaining a new incident VF; this risk increases with the number of prevalent fractures at the baseline and was proved to be BMD-independent (194,197). Conventional radiography and DXA represent the techniques of choice for VFs detection (198-200). Radiologic methods for the identification and the scoring of VFs include quantitative morphometry (QM), the visual semiquantitative (SQ) method and the "algorithm-based qualitative" (ABQ) method (8). QM was introduced in order to obtain an objective and reproducible evaluation of vertebral deformities based on the measurement of vertebral body heights. QM may be performed on conventional lateral spinal radiographs or on lateral spine views acquired by DXA; the densitometric approach is commonly termed as vertebral fracture assessment (VFA) (*Figure 5*) (201). Typically, the center of the superior and the inferior end plates and the corner points of each vertebra from T4 to L4 are identified and then these six points are used to calculate the anterior, the middle and the posterior heights (Ha, Hm and Hp, respectively) of each vertebra and the three height ratios (Ha/Hp for wedge fracture; Hm/Hp for biconcavity fractures; ratio between Hp of adjacent vertebrae for compression fractures) (*Figure 6*) (38). Today, the six points placement is performed automatically with the use of a dedicated computer-assisted system to avoid inter observer variability, but manual corrections are possible at any time during the post processing of the digital images (202). Point placement may be challenging due to normal variation in the shape of vertebral bodies and projection variations; moreover, QM does not allow to distinguish between real VFs and vertebral deformities (e.g., Scheuermann's disease, Schmorl's node, Cupid's bow deformity, etc.) (38,203). Unfortunately, at the current state of investigation, there is no gold standard for the definition of VFs and the exact degree of deformity that constitutes a fracture is still a matter of debate (203,204). In clinical trials, prevalent VFs are typically defined as a reduction of 3 SD or more (below the normative reference values for that particular vertebra) in any of the ratios of anterior, middle and posterior heights. In serial radiographs an incident fracture (i.e., a new VF) is defined both as an absolute change in vertebral height of at least 4 mm or as a percentage of reduction (15% or 20% reduction, depending on different studies) in the anterior, middle, or posterior heights from the baseline measurements (203,205).

The predominant approach for diagnosis of VFs is represented by the visual SQ method proposed by Genant *et al.* (206). On lateral spine images, VFs are identified on the basis of the apparent degree of vertebral

 

height loss (anterior, middle and/or posterior height) and/or projected area reduction estimated by visual inspection, without direct measurements (204,206). Vertebrae from T4 to L4 are graded as normal/not fractured (grade 0), mildly deformed (grade 1: 20–25% reduction in height; 10–20% reduction of projected vertebral area), moderately deformed (grade 2: 25–40% reduction in height and 20–40% reduction of projected vertebral area) and severely deformed (grade 3: >40% reduction in any height and projected vertebral area) (206). However over time, the area reduction requirement was excluded from the examination (205). Since a linear relationship exists between the number and severity of prevalent VFs and the risk of future VFs, a spinal deformity index (SDI) can be derived from this scoring system, resulting from the sum of all grades assigned to the vertebrae divided by the number of evaluated vertebrae (38,197). The SQ method has been extensively validated and according to the ISCD official positions it represents the technique of choice for diagnosing VFs with VFA (207,208,209). Its major strength relies on the visual approach that, in experienced hands, allows to discriminate fractures from non-fracture deformities (208,209). However, a critical point of this method is represented by the accurate estimation of vertebral height reduction, especially when the degree of this reduction is close to the thresholds of the grading system (204). In light of the above issues, we believe that an integrated approach may be preferable for defining and reporting VFs. In particular, the use of QM should be encouraged to objectively graduate VFs, previously identified by the SQ method, in epidemiological studies and follow up evaluations (202).

The ABQ is an alternative visual approach, recently developed and still waiting further validation for clinical practice. This method emphasizes the importance of visual inspection of the vertebral endplates to improve specificity in VFs detection (39). In the ABQ method the diagnosis of osteoporotic fractures is made on the basis of specific endplates abnormalities with depression of the central vertebral end-plate, regardless of vertebral height reduction; when a vertebra is reduced in height without endplate irregularities and texture changes below endplate (due to microfractures), this is classified as non-osteoporotic short vertebral height (SVH) (210). Using of this method, the prevalence of morphometric VFs could drop approximately of 30% (39). Jiang *et al.* documented a relatively poor agreement between SQ and ABQ methods for the identification of VFs ($\kappa$ =0.36) (211).

### *"Incidental" identification of VFs*

A discussed above, VFs frequently occur in absence of a major trauma and often remain asymptomatic; thus the majority of VFs are not clinically recognized at the time of their occurrence (212). Incidental diagnosis of VFs refers to the fortuitously identification of VFs in imaging examinations performed for other clinical purposes, such as chest and abdominal radiographs, CT and MRI that include visualization of the spine in their field of view (213). This represents a massive opportunity to gain additional information without the need for further scanning or radiation exposure, improving the management of patients at high risk of future osteoporotic fractures; nonetheless, there is significant underreporting of such fractures by radiologists (214). A possible explanation of this underreporting could be that, in reviewing CT and MRI performed for other clinical indications, intra-thoracic and/or intra-abdominal pathologies represent the main focus of the observer's attention; for this reason, a constant retraining of radiologists to emphasize the importance of VFs is required (214,215). Multidetector spiral CT of the thorax and abdomen is perhaps the most useful method for incidental VFs identification: on the midline sagittal CT reformations, the central area of the vertebral body end plate (the site where all VFs occur first) can be accurately analyzed allowing the detection of VFs not always evident on the transverse sections (214). Due to the growing number of CT and MRI examinations being routinely performed, the possible role of initial localizer views of CT (scout-CT) and MRI (MR-loc) for the detection of incidental VFs has recently been evaluated (195,213,216). The lateral scout CT view, preliminary acquired to define the anatomical area to be scanned, proved to be suitable to assess VFs (214,217). Intra-observer and inter-observer agreement based on a semiquantitative method are fair to good, with fractures of mild severity and fractures at the upper (T4–T9) thoracic levels representing the main sources of error (217,218). MR-loc images are a set of three-plane (axial, coronal and sagittal), low-resolution and large field-of-view images that serve to define the exact position and angulation of slices of MRI sequences; despite the limited image quality, MR-loc should be routinely scrutinized to search for incidental VFs that can be further confirmed by subsequently acquired T2-weighted sagittal images (213,214). MRI features also allow to discriminate between benign and malignant VFs and for the correct identification of recent and old vertebral compression fractures (219).

 

## Conclusions

Bone and muscle are two organs deeply related both in function and development, that conceptually constitute a unit, with interactions that take place at different levels from molecular to organic in a bidirectional way. Mechanical loading and muscle contraction are the most important determinants of bone mass and shape, with PA known to exert an anabolic effect on the metabolism of both bone and muscle. The development and the maintenance of bone mass and muscle mass are deeply related and both are affected by age and metabolic diseases.

Osteoporosis and sarcopenia represent two widespread diseases of increasing public interest, especially in the context of the rise of life expectancy, and represent an important area of geriatric and nutritional research. This review presents the different imaging modalities available for a non-invasive investigation of bone and muscle mass and quality in osteoporosis and sarcopenia, with special emphasis on the clinical application and limitations of each technique, and their potential complementary roles. In this regard, DXA is the most frequently utilized quantitative technique to investigate bone and skeletal muscles status in clinical practice, thanks to its wide availability, cost-effectiveness and low dose of ionizing radiation. In the field of osteoporosis, additional parameters, beyond BMD, can be extracted from DXA images; TBS and HAL have been extensively evaluated in research setting and have the potential to improve fracture risk prediction accuracy. The potential value of ultrasound for the prediction of fracture risk (QUS at the heel) and for the evaluation of muscle tissue has been well documented; however, the low reproducibility and difficulties in comparing measurements strongly limit its use. At the current state of knowledge, none of the operative definitions of sarcopenia include ultrasound in its diagnostic algorithm. Even if currently technically challenging and not widely available, in the future high-resolution imaging techniques will continue to expand our knowledge of the age, disease and treatment related changes that occur in bone and skeletal muscles.

## Acknowledgements

None.

## Footnote

*Conflicts of Interest*: The authors have no conflicts of interest to declare.

## References

1. Laurent MR, Dubois V, Claessens F, Verschueren SM, Vanderschueren D, Gielen E, Jardí F. Muscle-bone interactions: From experimental models to the clinic? A critical update. Mol Cell Endocrinol 2016;432:14-36.
2. Tagliaferri C, Wittrant Y, Davicco MJ, Walrand S, Coxam V. Muscle and bone, two interconnected tissues. Ageing Res Rev 2015;21:55-70.
3. Frost HM. Bone "mass" and the "mechanostat": a proposal. Anat Rec 1987;219:1-9.
4. Frost HM. Bone's mechanostat: a 2003 update. Anat Rec A Discov Mol Cell Evol Biol 2003;275:1081-101.
5. Ferretti JL, Capozza RF, Cointry GR, Garcia SL, Plotkin H, Alvarez Filgueira ML, Zanchetta JR. Gender-related differences in the relationship between densitometric values of whole-body bone mineral content and lean body mass in humans between 2 and 87 years of age. Bone 1998;22:683-90.
6. Andreoli A, Bazzocchi A, Celi M, Lauro D, Sorge R, Tarantino U, Guglielmi G. Relationship between body composition, body mass index and bone mineral density in a large population of normal, osteopenic and osteoporotic women. Radiol Med 2011;116:1115-23.
7. Erlandson MC, Lorbergs AL, Mathur S, Cheung AM. Muscle analysis using pQCT, DXA and MRI. Eur J Radiol 2016;85:1505-11.
8. Oei L, Koromani F, Rivadeneira F, Zillikens MC, Oei EH. Quantitative imaging methods in osteoporosis. Quant Imaging Med Surg 2016;6:680-98.
9. NIH Consensus Development Panel on Osteoporosis Prevention, Diagnosis, and Therapy. Osteoporosis prevention, diagnosis, and therapy. JAMA 2001;285:785-95.
10. Fonseca H, Moreira-Goncalves D, Coriolano HJ, Duarte JA. Bone quality: the determinants of bone strength and fragility. Sports Med 2014;44:37-53.
11. Turner CH. Bone strength: current concepts. Ann N Y Acad Sci 2006;1068:429-46.
12. Hernlund E, Svedbom A, Ivergård M, Compston J, Cooper C, Stenmark J, McCloskey EV, Jönsson B, Kanis JA. Osteoporosis in the European Union: medical management, epidemiology and economic burden. Arch Osteoporos 2013;8:136.
13. Wright NC, Looker AC, Saag KG, Curtis JR, Delzell ES, Randall S, Dawson-Hughes B. The recent prevalence of osteoporosis and low bone mass in the United States based

 

on bone mineral density at the femoral neck or lumbar spine. J Bone Miner Res 2014;29:2520-6.
14. Budhia S, Mikyas Y, Tang M, Badamgarav E. Osteoporotic fractures: a systematic review of U.S. healthcare costs and resource utilization. Pharmacoeconomics 2012;30:147-70.
15. Burge R, Dawson-Hughes B, Solomon DH, Wong JB, King A, Tosteson A. Incidence and economic burden of osteoporosis-related fractures in the United States, 2005-2025. J Bone Miner Res 2007;22:465-75.
16. Rosenberg IH. Summary comments. Am J Clin Nutr 1989;50:1231-3.
17. Cruz-Jentoft AJ, Baeyens JP, Bauer JM, Boirie Y, Cederholm T, Landi F, Martin FC, Michel JP, Rolland Y, Schneider SM, Topinkova E, Vandewoude M, Zamboni M. Sarcopenia: European consensus on definition and diagnosis: Report of the European Working Group on Sarcopenia in Older People. Age Ageing 2010;39:412-23.
18. Beaudart C, Rizzoli R, Bruyère O, Reginster JY, Biver E. Sarcopenia: burden and challenges for public health. Arch Public Health 2014;72:45.
19. Cruz-Jentoft AJ, Landi F, Schneider SM, Zuniga C, Arai H, Boirie Y, Chen LK, Fielding RA, Martin FC, Michel JP, Sieber C, Stout JR, Studenski SA, Vellas B, Woo J, Zamboni M, Cederholm T. Prevalence of and interventions for sarcopenia in ageing adults: a systematic review. Report of the International Sarcopenia Initiative (EWGSOP and IWGS). Age Ageing 2014;43:748-59.
20. Dennison EM, Sayer AA, Cooper C. Epidemiology of sarcopenia and insight into possible therapeutic targets. Nat Rev Rheumatol 2017;13:340-7.
21. Reginster JY, Beaudart C, Buckinx F, Bruyere O. Osteoporosis and sarcopenia: two diseases or one? Curr Opin Clin Nutr Metab Care 2016;19:31-6.
22. Janssen I, Shepard DS, Katzmarzyk PT, Roubenoff R. The healthcare costs of sarcopenia in the United States. J Am Geriatr Soc 2004;52:80-5.
23. Curtis E, Litwic A, Cooper C, Dennison E. Determinants of Muscle and Bone Aging. J Cell Physiol 2015;230:2618-25.
24. Lang T, Streeper T, Cawthon P, Baldwin K, Taaffe DR, Harris TB. Sarcopenia: etiology, clinical consequences, intervention, and assessment. Osteoporos Int 2010;21:543-59.
25. Hamrick MW, McGee-Lawrence ME, Frechette DM. Fatty Infiltration of Skeletal Muscle: Mechanisms and Comparisons with Bone Marrow Adiposity. Front Endocrinol (Lausanne) 2016;7:69.
26. Bermeo S, Gunaratnam K, Duque G. Fat and bone interactions. Curr Osteoporos Rep 2014;12:235-42.
27. Rosen CJ, Ackert-Bicknell C, Rodriguez JP, Pino AM. Marrow fat and the bone microenvironment: developmental, functional, and pathological implications. Crit Rev Eukaryot Gene Expr 2009;19:109-24.
28. Verma S, Rajaratnam JH, Denton J, Hoyland JA, Byers RJ. Adipocytic proportion of bone marrow is inversely related to bone formation in osteoporosis. J Clin Pathol 2002;55:693-8.
29. Ponti F, Guerri S, Sassi C, Battista G, Guglielmi G, Bazzocchi A. Imaging of diabetic bone. Endocrine 2017;58:426-41.
30. Reinders I, Murphy RA, Brouwer IA, Visser M, Launer L, Siggeirsdottir K, Eiriksdottir G, Gudnason V, Jonsson PV, Lang TF, Harris TB. Muscle Quality and Myosteatosis: Novel Associations With Mortality Risk: The Age, Gene/Environment Susceptibility (AGES)-Reykjavik Study. Am J Epidemiol 2016;183:53-60.
31. Tuttle LJ, Sinacore DR, Mueller MJ. Intermuscular Adipose Tissue Is Muscle Specific and Associated with Poor Functional Performance. J Aging Res 2012;2012:172957.
32. Cauley JA. An Overview of Sarcopenic Obesity. J Clin Densitom 2015;18:499-505.
33. Lang T, Cauley JA, Tylavsky F, Bauer D, Cummings S, Harris TB. Computed tomographic measurements of thigh muscle cross-sectional area and attenuation coefficient predict hip fracture: the health, aging, and body composition study. J Bone Miner Res 2010;25:513-9.
34. Guideline for the prevention of falls in older persons. American Geriatrics Society, British Geriatrics Society, and American Academy of Orthopaedic Surgeons Panel on Falls Prevention. J Am Geriatr Soc 2001;49:664-72.
35. Rubenstein LZ. Falls in older people: epidemiology, risk factors and strategies for prevention. Age Ageing 2006;35:ii37-41.
36. Rubenstein LZ, Josephson KR. The epidemiology of falls and syncope. Clin Geriatr Med 2002;18:141-58.
37. Yu SC, Khow KS, Jadczak AD, Visvanathan R. Clinical Screening Tools for Sarcopenia and Its Management. Curr Gerontol Geriatr Res 2016;2016:5978523.
38. Guglielmi G, Muscarella S, Bazzocchi A. Integrated imaging approach to osteoporosis: state-of-the-art review and update. Radiographics 2011;31:1343-64.
39. Anil G, Guglielmi G, Peh WC. Radiology of osteoporosis. Radiol Clin North Am 2010;48:497-518.
40. Singh M, Nagrath AR, Maini PS. Changes in trabecular pattern of the upper end of the femur as an index of osteoporosis. J Bone Joint Surg Am 1970;52:457-67.

 

41. Singh M, Riggs BL, Beabout JW, Jowsey J. Femoral trabecular-pattern index for evaluation of spinal osteoporosis. Ann Intern Med 1972;77:63-7.
42. Jhamaria NL, Lal KB, Udawat M, Banerji P, Kabra SG. The trabecular pattern of the calcaneum as an index of osteoporosis. J Bone Joint Surg Br 1983;65:195-8.
43. Adams JE. Radiogrammetry and radiographic absorptiometry. Radiol Clin North Am 2010;48:531-40.
44. Mack PB, O'Brien A T, Smith JM, Bauman AW. A method for estimating the degree of mineralization of bones from tracings of roentgenograms. Science 1939;89:467.
45. Cosman F, Herrington B, Himmelstein S, Lindsay R. Radiographic absorptiometry: a simple method for determination of bone mass. Osteoporos Int 1991;2:34-8.
46. Hyldstrup L, Nielsen SP. Metacarpal Index by Digital X-ray Radiogrammetry: Normative Reference Values and Comparison with Dual X-ray Absorptiometry. J Clin Densitom 2001;4:299-306.
47. Barnett E, Nordin BE. The radiological diagnosis of osteoporosis: a new approach. Clin Radiol 1960;11:166-74.
48. Rosholm A, Hyldstrup L, Bæksgaard L, Grunkin M, Thodberg HH. Estimation of Bone Mineral Density by Digital X-ray Radiogrammetry: Theoretical Background and Clinical Testing. Osteoporos Int 2001;12:961-9.
49. Bazzocchi A, Ponti F, Albisinni U, Battista G, Guglielmi G. DXA: Technical aspects and application. Eur J Radiol 2016;85:1481-92.
50. Guglielmi G, Bazzocchi A. Editorial. Eur J Radiol 2016;85:1453-5.
51. Bazzocchi A, Ciccarese F, Diano D, Spinnato P, Albisinni U, Rossi C, Guglielmi G. Dual-energy X-ray absorptiometry in the evaluation of abdominal aortic calcifications. J Clin Densitom 2012;15:198-204.
52. Bazzocchi A, Diano D. Dual-energy X-ray absorptiometry in obesity. CMAJ 2014;186:48.
53. Bazzocchi A, Diano D, Albisinni U, Marchesini G, Battista G, Guglielmi G. Liver in the analysis of body composition by dual-energy X-ray absorptiometry. Br J Radiol 2014;87:20140232.
54. Bazzocchi A, Diano D, Ponti F, Andreone A, Sassi C, Albisinni U, Marchesini G, Battista G. Health and ageing: a cross-sectional study of body composition. Clin Nutr 2013;32:569-78.
55. Bazzocchi A, Diano D, Ponti F, Salizzoni E, Albisinni U, Marchesini G, Battista G. A 360-degree overview of body composition in healthy people: relationships among anthropometry, ultrasonography, and dual-energy x-ray absorptiometry. Nutrition 2014;30:696-701.
56. Bazzocchi A, Diano D, Vicennati V, Pizzi C, De Filippo M, Pasquali R, Rossi C, Battista G. Relationships between total and regional adiposity and epicardial fat in obese women: how can dual-energy X-ray absorptiometry be associated with echocardiographic epicardial fat measurements? Clin Obes 2013;3:132-40.
57. Bazzocchi A, Ferrari F, Diano D, Albisinni U, Battista G, Rossi C, Guglielmi G. Incidental findings with dual-energy X-ray absorptiometry: spectrum of possible diagnoses. Calcif Tissue Int 2012;91:149-56.
58. Bazzocchi A, Ponti F, Cariani S, Diano D, Leuratti L, Albisinni U, Marchesini G, Battista G. Visceral fat and body composition changes in a female population after RYGBP: a two-year follow-up by DXA. Obes Surg 2015;25:443-51.
59. Pelusi C, Costantino A, Martelli V, Lambertini M, Bazzocchi A, Ponti F, Battista G, Venturoli S, Meriggiola MC. Effects of three different testosterone formulations in female-to-male transsexual persons. J Sex Med 2014;11:3002-11.
60. Franzoni E, Ciccarese F, Di Pietro E, Facchini G, Moscano F, Iero L, Monaldi A, Battista G, Bazzocchi A. Follow-up of bone mineral density and body composition in adolescents with restrictive anorexia nervosa: role of dual-energy X-ray absorptiometry. Eur J Clin Nutr 2014;68:247-52.
61. Pietrobelli A, Formica C, Wang Z, Heymsfield SB. Dual-energy X-ray absorptiometry body composition model: review of physical concepts. Am J Physiol 1996;271:E941-51.
62. Toombs RJ, Ducher G, Shepherd JA, De Souza MJ. The impact of recent technological advances on the trueness and precision of DXA to assess body composition. Obesity 2012;20:30-9.
63. Assessment of fracture risk and its application to screening for postmenopausal osteoporosis. Report of a WHO Study Group. World Health Organ Tech Rep Ser 1994;843:1-129.
64. Messina C, Bignotti B, Bazzocchi A, Phan CM, Tagliafico A, Guglielmi G, Sardanelli F, Sconfienza LM. A critical appraisal of the quality of adult dual-energy X-ray absorptiometry guidelines in osteoporosis using the AGREE II tool: An EuroAIM initiative. Insights Imaging 2017;8:311-7.
65. Schousboe JT, Shepherd JA, Bilezikian JP, Baim S. Executive summary of the 2013 International Society for Clinical Densitometry Position Development Conference on bone densitometry. J Clin Densitom 2013;16:455-66.
66. Hawkinson J, Timins J, Angelo D, Shaw M, Takata R, Harshaw F. Technical white paper: bone densitometry. J Am Coll Radiol 2007;4:320-7.

 

67. Kalender WA. Effective dose values in bone mineral measurements by photon absorptiometry and computed tomography. Osteoporos Int 1992;2:82-7.
68. Wall BF, Hart D. Revised radiation doses for typical X-ray examinations. Report on a recent review of doses to patients from medical X-ray examinations in the UK by NRPB. National Radiological Protection Board. Br J Radiol 1997;70:437-9.
69. Hordon LD, Raisi M, Aaron JE, Paxton SK, Beneton M, Kanis JA. Trabecular architecture in women and men of similar bone mass with and without vertebral fracture: I. Two-dimensional histology. Bone 2000;27:271-6.
70. Johnell O, Kanis JA, Oden A, Johansson H, De Laet C, Delmas P, Eisman JA, Fujiwara S, Kroger H, Mellstrom D, Meunier PJ, Melton LJ 3rd, O'Neill T, Pols H, Reeve J, Silman A, Tenenhouse A. Predictive value of BMD for hip and other fractures. J Bone Miner Res 2005;20:1185-94.
71. Ammann P, Rizzoli R. Bone strength and its determinants. Osteoporos Int 2003;14:S13-8.
72. Janghorbani M, Van Dam RM, Willett WC, Hu FB. Systematic review of type 1 and type 2 diabetes mellitus and risk of fracture. Am J Epidemiol 2007;166:495-505.
73. Vestergaard P. Discrepancies in bone mineral density and fracture risk in patients with type 1 and type 2 diabetes--a meta-analysis. Osteoporos Int 2007;18:427-44.
74. Oei L, Zillikens MC, Dehghan A, Buitendijk GH, Castano-Betancourt MC, Estrada K, Stolk L, Oei EH, van Meurs JB, Janssen JA, Hofman A, van Leeuwen JP, Witteman JC, Pols HA, Uitterlinden AG, Klaver CC, Franco OH, Rivadeneira F. High bone mineral density and fracture risk in type 2 diabetes as skeletal complications of inadequate glucose control: the Rotterdam Study. Diabetes Care 2013;36:1619-28.
75. de Liefde II, van der Klift M, de Laet CE, van Daele PL, Hofman A, Pols HA. Bone mineral density and fracture risk in type-2 diabetes mellitus: the Rotterdam Study. Osteoporos Int 2005;16:1713-20.
76. Granchi D, Caudarella R, Ripamonti C, Spinnato P, Bazzocchi A, Torreggiani E, Massa A, Baldini N. Association between markers of bone loss and urinary lithogenic risk factors in osteopenic postmenopausal women. J Biol Regul Homeost Agents 2016;30:145-51.
77. Harvey NC, Gluer CC, Binkley N, McCloskey EV, Brandi ML, Cooper C, Kendler D, Lamy O, Laslop A, Camargos BM, Reginster JY, Rizzoli R, Kanis JA. Trabecular bone score (TBS) as a new complementary approach for osteoporosis evaluation in clinical practice. Bone 2015;78:216-24.
78. Pothuaud L, Carceller P, Hans D. Correlations between grey-level variations in 2D projection images (TBS) and 3D microarchitecture: applications in the study of human trabecular bone microarchitecture. Bone 2008;42:775-87.
79. Silva BC, Leslie WD, Resch H, Lamy O, Lesnyak O, Binkley N, McCloskey EV, Kanis JA, Bilezikian JP. Trabecular bone score: a noninvasive analytical method based upon the DXA image. J Bone Miner Res 2014;29:518-30.
80. Hans D, Barthe N, Boutroy S, Pothuaud L, Winzenrieth R, Krieg MA. Correlations between trabecular bone score, measured using anteroposterior dual-energy X-ray absorptiometry acquisition, and 3-dimensional parameters of bone microarchitecture: an experimental study on human cadaver vertebrae. J Clin Densitom 2011;14:302-12.
81. Silva BC, Broy SB, Boutroy S, Schousboe JT, Shepherd JA, Leslie WD. Fracture Risk Prediction by Non-BMD DXA Measures: the 2015 ISCD Official Positions Part 2: Trabecular Bone Score. J Clin Densitom 2015;18:309-30.
82. Hans D, Goertzen AL, Krieg MA, Leslie WD. Bone microarchitecture assessed by TBS predicts osteoporotic fractures independent of bone density: the Manitoba study. J Bone Miner Res 2011;26:2762-9.
83. Leslie WD, Aubry-Rozier B, Lamy O, Hans D. TBS (trabecular bone score) and diabetes-related fracture risk. J Clin Endocrinol Metab 2013;98:602-9.
84. Ulivieri FM, Silva BC, Sardanelli F, Hans D, Bilezikian JP, Caudarella R. Utility of the trabecular bone score (TBS) in secondary osteoporosis. Endocrine 2014;47:435-48.
85. Bazzocchi A, Ponti F, Diano D, Amadori M, Albisinni U, Battista G, Guglielmi G. Trabecular bone score in healthy ageing. Br J Radiol 2015;88:20140865.
86. Beck TJ. Extending DXA beyond bone mineral density: understanding hip structure analysis. Curr Osteoporos Rep 2007;5:49-55.
87. Bonnick SL. HSA: beyond BMD with DXA. Bone 2007;41:S9-12.
88. Broy SB, Cauley JA, Lewiecki ME, Schousboe JT, Shepherd JA, Leslie WD. Fracture Risk Prediction by Non-BMD DXA Measures: the 2015 ISCD Official Positions Part 1: Hip Geometry. J Clin Densitom 2015;18:287-308.
89. Faulkner KG, Cummings SR, Black D, Palermo L, Gluer CC, Genant HK. Simple measurement of femoral geometry predicts hip fracture: the study of osteoporotic fractures. J Bone Miner Res 1993;8:1211-7.
90. Leslie WD, Lix LM, Morin SN, Johansson H, Oden A, McCloskey EV, Kanis JA. Hip axis length is a FRAX- and

 

bone density-independent risk factor for hip fracture in women. J Clin Endocrinol Metab 2015;100:2063-70.
91. Leslie WD, Lix LM, Morin SN, Johansson H, Oden A, McCloskey EV, Kanis JA. Adjusting Hip Fracture Probability in Men and Women Using Hip Axis Length: the Manitoba Bone Density Database. J Clin Densitom 2016;19:326-31.
92. Levine JA, Abboud L, Barry M, Reed JE, Sheedy PF, Jensen MD. Measuring leg muscle and fat mass in humans: comparison of CT and dual-energy X-ray absorptiometry. J Appl Physiol (1985) 2000;88:452-6.
93. Maden-Wilkinson TM, Degens H, Jones DA, McPhee JS. Comparison of MRI and DXA to measure muscle size and age-related atrophy in thigh muscles. J Musculoskelet Neuronal Interact 2013;13:320-8.
94. Guglielmi G, Ponti F, Agostini M, Amadori M, Battista G, Bazzocchi A. The role of DXA in sarcopenia. Aging Clin Exp Res 2016;28:1047-60.
95. Janssen I, Heymsfield SB, Ross R. Low relative skeletal muscle mass (sarcopenia) in older persons is associated with functional impairment and physical disability. J Am Geriatr Soc 2002;50:889-96.
96. Shepherd JA, Baim S, Bilezikian JP, Schousboe JT. Executive summary of the 2013 International Society for Clinical Densitometry Position Development Conference on Body Composition. J Clin Densitom 2013;16:489-95.
97. Coin A, Giannini S, Minicuci N, Rinaldi G, Pedrazzoni M, Minisola S, Rossini M, Del Puente A, Inelmen EM, Manzato E, Sergi G. Limb fat-free mass and fat mass reference values by dual-energy X-ray absorptiometry (DEXA) in a 20-80 year-old Italian population. Clin Nutr 2012;31:506-11.
98. Xiao Z, Guo B, Gong J, Tang Y, Shang J, Cheng Y, Xu H. Sex- and age-specific percentiles of body composition indices for Chinese adults using dual-energy X-ray absorptiometry. Eur J Nutr 2017;56:2393-406.
99. Diano D, Ponti F, Guerri S, Mercatelli D, Amadori M, Aparisi Gomez MP, Battista G, Guglielmi G, Bazzocchi A. Upper and lower limbs composition: a comparison between anthropometry and dual-energy X-ray absorptiometry in healthy people. Arch Osteoporos 2017;12:78.
100. Clark P, Denova-Gutierrez E, Ambrosi R, Szulc P, Rivas-Ruiz R, Salmeron J. Reference Values of Total Lean Mass, Appendicular Lean Mass, and Fat Mass Measured with Dual-Energy X-ray Absorptiometry in a Healthy Mexican Population. Calcif Tissue Int 2016;99:462-71.
101. Gould H, Brennan SL, Kotowicz MA, Nicholson GC, Pasco JA. Total and appendicular lean mass reference ranges for Australian men and women: the Geelong osteoporosis study. Calcif Tissue Int 2014;94:363-72.
102. Krug R, Burghardt AJ, Majumdar S, Link TM. High-resolution imaging techniques for the assessment of osteoporosis. Radiol Clin North Am 2010;48:601-21.
103. Genant HK, Block JE, Steiger P, Glueer CC, Smith R. Quantitative computed tomography in assessment of osteoporosis. Semin Nucl Med 1987;17:316-33.
104. D'Elia G, Caracchini G, Cavalli L, Innocenti P. Bone fragility and imaging techniques. Clin Cases Miner Bone Metab 2009;6:234-46.
105. Engelke K, Adams JE, Armbrecht G, Augat P, Bogado CE, Bouxsein ML, Felsenberg D, Ito M, Prevrhal S, Hans DB, Lewiecki EM. Clinical use of quantitative computed tomography and peripheral quantitative computed tomography in the management of osteoporosis in adults: the 2007 ISCD Official Positions. J Clin Densitom 2008;11:123-62.
106. Li N, Li XM, Xu L, Sun WJ, Cheng XG, Tian W. Comparison of QCT and DXA: Osteoporosis Detection Rates in Postmenopausal Women. Int J Endocrinol 2013;2013:895474.
107. Genant HK, Engelke K, Prevrhal S. Advanced CT bone imaging in osteoporosis. Rheumatology (Oxford) 2008;47 Suppl 4:iv9-16.
108. Engelke K, Lang T, Khosla S, Qin L, Zysset P, Leslie WD, Shepherd JA, Shousboe JT. Clinical Use of Quantitative Computed Tomography-Based Advanced Techniques in the Management of Osteoporosis in Adults: the 2015 ISCD Official Positions-Part III. J Clin Densitom 2015;18:393-407.
109. Stagi S, Cavalli L, Cavalli T, de Martino M, Brandi ML. Peripheral quantitative computed tomography (pQCT) for the assessment of bone strength in most of bone affecting conditions in developmental age: a review. Ital J Pediatr 2016;42:88.
110. Engelke K, Lang T, Khosla S, Qin L, Zysset P, Leslie WD, Shepherd JA, Schousboe JT. Clinical Use of Quantitative Computed Tomography (QCT) of the Hip in the Management of Osteoporosis in Adults: the 2015 ISCD Official Positions-Part I. J Clin Densitom 2015;18:338-58.
111. Issever AS, Link TM, Kentenich M, Rogalla P, Burghardt AJ, Kazakia GJ, Majumdar S, Diederichs G. Assessment of trabecular bone structure using MDCT: comparison of 64- and 320-slice CT using HR-pQCT as the reference standard. Eur Radiol 2010;20:458-68.
112. Griffith JF, Genant HK. New advances in imaging osteoporosis and its complications. Endocrine

 

2012;42:39-51.
113. Liu XS, Cohen A, Shane E, Yin PT, Stein EM, Rogers H, Kokolus SL, McMahon DJ, Lappe JM, Recker RR, Lang T, Guo XE. Bone density, geometry, microstructure, and stiffness: Relationships between peripheral and central skeletal sites assessed by DXA, HR-pQCT, and cQCT in premenopausal women. J Bone Miner Res 2010;25:2229-38.
114. Nishiyama KK, Shane E. Clinical Imaging of Bone Microarchitecture with HR-pQCT. Curr Osteoporos Rep 2013;11:147-55.
115. Burghardt AJ, Kazakia GJ, Link TM, Majumdar S. Automated simulation of areal bone mineral density assessment in the distal radius from high-resolution peripheral quantitative computed tomography. Osteoporos Int 2009;20:2017-24.
116. Liu XS, Sajda P, Saha PK, Wehrli FW, Bevill G, Keaveny TM, Guo XE. Complete volumetric decomposition of individual trabecular plates and rods and its morphological correlations with anisotropic elastic moduli in human trabecular bone. J Bone Miner Res 2008;23:223-35.
117. Stein EM, Silva BC, Boutroy S, Zhou B, Wang J, Udesky J, Zhang C, McMahon DJ, Romano M, Dworakowski E, Costa AG, Cusano N, Irani D, Cremers S, Shane E, Guo XE, Bilezikian JP. Primary Hyperparathyroidism is Associated with Abnormal Cortical and Trabecular Microstructure and Reduced Bone Stiffness in Postmenopausal Women. J Bone Miner Res 2013;28:1029-40.
118. Patsch JM, Burghardt AJ, Yap SP, Baum T, Schwartz AV, Joseph GB, Link TM. Increased cortical porosity in type 2 diabetic postmenopausal women with fragility fractures. J Bone Miner Res 2013;28:313-24.
119. Burghardt AJ, Issever AS, Schwartz AV, Davis KA, Masharani U, Majumdar S, Link TM. High-resolution peripheral quantitative computed tomographic imaging of cortical and trabecular bone microarchitecture in patients with type 2 diabetes mellitus. J Clin Endocrinol Metab 2010;95:5045-55.
120. Goodpaster BH, Thaete FL, Kelley DE. Composition of skeletal muscle evaluated with computed tomography. Ann N Y Acad Sci 2000;904:18-24.
121. Ross R. Advances in the application of imaging methods in applied and clinical physiology. Acta Diabetol 2003;40:S45-50.
122. Mitsiopoulos N, Baumgartner RN, Heymsfield SB, Lyons W, Gallagher D, Ross R. Cadaver validation of skeletal muscle measurement by magnetic resonance imaging and computerized tomography. J Appl Physiol 1998;85:115-22.
123. Wong AK, Hummel K, Moore C, Beattie KA, Shaker S, Craven BC, Adachi JD, Papaioannou A, Giangregorio L. Improving Reliability of pQCT-Derived Muscle Area and Density Measures Using a Watershed Algorithm for Muscle and Fat Segmentation. J Clin Densitom 2015;18:93-101.
124. Houmard JA, Smith R, Jendrasiak GL. Relationship between MRI relaxation time and muscle fiber composition. J Appl Physiol (1985) 1995;78:807-9.
125. Majumdar S. Magnetic resonance imaging of trabecular bone structure. Top Magn Reson Imaging 2002;13:323-34.
126. Majumdar S, Newitt D, Jergas M, Gies A, Chiu E, Osman D, Keltner J, Keyak J, Genant H. Evaluation of technical factors affecting the quantification of trabecular bone structure using magnetic resonance imaging. Bone 1995;17:417-30.
127. Majumdar S, Genant HK. A review of the recent advances in magnetic resonance imaging in the assessment of osteoporosis. Osteoporos Int 1995;5:79-92.
128. Adams JE. Advances in bone imaging for osteoporosis. Nat Rev Endocrinol 2013;9:28-42.
129. Link TM, Majumdar S, Lin JC, Newitt D, Augat P, Ouyang X, Mathur A, Genant HK. A comparative study of trabecular bone properties in the spine and femur using high resolution MRI and CT. J Bone Miner Res 1998;13:122-32.
130. Krug R, Banerjee S, Han ET, Newitt DC, Link TM, Majumdar S. Feasibility of in vivo structural analysis of high-resolution magnetic resonance images of the proximal femur. Osteoporos Int 2005;16:1307-14.
131. Krug R, Carballido-Gamio J, Burghardt AJ, Kazakia G, Hyun BH, Jobke B, Banerjee S, Huber M, Link TM, Majumdar S. Assessment of trabecular bone structure comparing magnetic resonance imaging at 3 Tesla with high-resolution peripheral quantitative computed tomography ex vivo and in vivo. Osteoporos Int 2008;19:653-61.
132. Link TM, Vieth V, Stehling C, Lotter A, Beer A, Newitt D, Majumdar S. High-resolution MRI vs multislice spiral CT: which technique depicts the trabecular bone structure best? Eur Radiol 2003;13:663-71.
133. Sell CA, Masi JN, Burghardt A, Newitt D, Link TM, Majumdar S. Quantification of trabecular bone structure using magnetic resonance imaging at 3 Tesla--calibration studies using microcomputed tomography as a standard of reference. Calcif Tissue Int 2005;76:355-64.
134. Majumdar S. Magnetic resonance imaging for osteoporosis. Skeletal Radiol 2008;37:95-7.

 

135. Majumdar S, Link TM, Augat P, Lin JC, Newitt D, Lane NE, Genant HK. Trabecular bone architecture in the distal radius using magnetic resonance imaging in subjects with fractures of the proximal femur. Magnetic Resonance Science Center and Osteoporosis and Arthritis Research Group. Osteoporos Int 1999;10:231-9.
136. Link TM, Majumdar S, Augat P, Lin JC, Newitt D, Lu Y, Lane NE, Genant HK. In vivo high resolution MRI of the calcaneus: differences in trabecular structure in osteoporosis patients. J Bone Miner Res 1998;13:1175-82.
137. Wehrli FW, Gomberg BR, Saha PK, Song HK, Hwang SN, Snyder PJ. Digital topological analysis of in vivo magnetic resonance microimages of trabecular bone reveals structural implications of osteoporosis. J Bone Miner Res 2001;16:1520-31.
138. Chang G, Wang L, Liang G, Babb JS, Wiggins GC, Saha PK, Regatte RR. Quantitative assessment of trabecular bone micro-architecture of the wrist via 7 Tesla MRI: preliminary results. MAGMA 2011;24:191-9.
139. Guenoun D, Foure A, Pithioux M, Guis S, Le Corroller T, Mattei JP, Pauly V, Guye M, Bernard M, Chabrand P, Champsaur P, Bendahan D. Correlative Analysis of Vertebral Trabecular Bone Microarchitecture and Mechanical Properties: A Combined Ultra-high Field (7 Tesla) MRI and Biomechanical Investigation. Spine 2017;42:E1165-72.
140. Fazeli PK, Horowitz MC, MacDougald OA, Scheller EL, Rodeheffer MS, Rosen CJ, Klibanski A. Marrow fat and bone--new perspectives. J Clin Endocrinol Metab 2013;98:935-45.
141. Schellinger D, Lin CS, Lim J, Hatipoglu HG, Pezzullo JC, Singer AJ. Bone marrow fat and bone mineral density on proton MR spectroscopy and dual-energy X-ray absorptiometry: their ratio as a new indicator of bone weakening. AJR Am J Roentgenol 2004;183:1761-5.
142. Yeung DK, Griffith JF, Antonio GE, Lee FK, Woo J, Leung PC. Osteoporosis is associated with increased marrow fat content and decreased marrow fat unsaturation: a proton MR spectroscopy study. J Magn Reson Imaging 2005;22:279-85.
143. Boutin RD, Yao L, Canter RJ, Lenchik L. Sarcopenia: Current Concepts and Imaging Implications. AJR Am J Roentgenol 2015;205:W255-66.
144. Abellan van Kan G, Cderbaum JM, Cesari M, Dahinden P, Fariello RG, Fielding RA, Goodpaster BH, Hettwer S, Isaac M, Laurent D, Morley JE, Pahor M, Rooks D, Roubenoff R, Rutkove SB, Shaheen A, Vamvakas S, Vrijbloed JW, Vellas B. Sarcopenia: biomarkers and imaging (International Conference on Sarcopenia research). J Nutr Health Aging 2011;15:834-46.
145. Fischer MA, Pfirrmann CW, Espinosa N, Raptis DA, Buck FM. Dixon-based MRI for assessment of muscle-fat content in phantoms, healthy volunteers and patients with achillodynia: comparison to visual assessment of calf muscle quality. Eur Radiol 2014;24:1366-75.
146. Alizai H, Nardo L, Karampinos DC, Joseph GB, Yap SP, Baum T, Krug R, Majumdar S, Link TM. Comparison of clinical semi-quantitative assessment of muscle fat infiltration with quantitative assessment using chemical shift-based water/fat separation in MR studies of the calf of post-menopausal women. Eur Radiol 2012;22:1592-600.
147. Nardo L, Karampinos DC, Lansdown DA, Carballido-Gamio J, Lee S, Maroldi R, Ma CB, Link TM, Krug R. Quantitative assessment of fat infiltration in the rotator cuff muscles using water-fat MRI. J Magn Reson Imaging 2014;39:1178-85.
148. Cao P, Fan SJ, Wang AM, Xie VB, Qiao Z, Brittenham GM, Wu EX. Diffusion magnetic resonance monitors intramyocellular lipid droplet size in vivo. Magn Reson Med 2015;73:59-69.
149. Hu HH, Kan HE. Quantitative proton MR techniques for measuring fat. NMR Biomed 2013;26:1609-29.
150. Kuhlmann J, Neumann-Haefelin C, Belz U, Kalisch J, Juretschke HP, Stein M, Kleinschmidt E, Kramer W, Herling AW. Intramyocellular lipid and insulin resistance: a longitudinal in vivo 1H-spectroscopic study in Zucker diabetic fatty rats. Diabetes 2003;52:138-44.
151. Janssen I, Heymsfield SB, Wang ZM, Ross R. Skeletal muscle mass and distribution in 468 men and women aged 18-88 yr. J Appl Physiol 2000;89:81-8.
152. Kent-Braun JA, Ng AV, Young K. Skeletal muscle contractile and noncontractile components in young and older women and men. J Appl Physiol (1985) 2000;88:662-8.
153. Macaluso A, Nimmo MA, Foster JE, Cockburn M, McMillan NC, De Vito G. Contractile muscle volume and agonist-antagonist coactivation account for differences in torque between young and older women. Muscle Nerve 2002;25:858-63.
154. Nilwik R, Snijders T, Leenders M, Groen BB, van Kranenburg J, Verdijk LB, van Loon LJ. The decline in skeletal muscle mass with aging is mainly attributed to a reduction in type II muscle fiber size. Exp Gerontol 2013;48:492-8.
155. Ticinesi A, Meschi T, Narici MV, Lauretani F, Maggio M. Muscle Ultrasound and Sarcopenia in Older Individuals: A

 

Clinical Perspective. J Am Med Dir Assoc 2017;18:290-300.
156. Gluer CC. Quantitative ultrasound techniques for the assessment of osteoporosis: expert agreement on current status. The International Quantitative Ultrasound Consensus Group. J Bone Miner Res 1997;12:1280-8.
157. Guglielmi G, Scalzo G, de Terlizzi F, Peh WC. Quantitative ultrasound in osteoporosis and bone metabolism pathologies. Radiol Clin North Am 2010;48:577-88.
158. Krieg MA, Barkmann R, Gonnelli S, Stewart A, Bauer DC, Del Rio Barquero L, Kaufman JJ, Lorenc R, Miller PD, Olszynski WP, Poiana C, Schott AM, Lewiecki EM, Hans D. Quantitative ultrasound in the management of osteoporosis: the 2007 ISCD Official Positions. J Clin Densitom 2008;11:163-87.
159. Krieg MA, Thiebaud D, Landry M, Burckhardt P. Evaluation of bones using quantitative ultrasonography. Schweiz Med Wochenschr 1996;126:159-63.
160. Roux C, Fournier B, Laugier P, Chappard C, Kolta S, Dougados M, Berger G. Broadband ultrasound attenuation imaging: a new imaging method in osteoporosis. J Bone Miner Res 1996;11:1112-8.
161. Hans D, Dargent-Molina P, Schott AM, Sebert JL, Cormier C, Kotzki PO, Delmas PD, Pouilles JM, Breart G, Meunier PJ. Ultrasonographic heel measurements to predict hip fracture in elderly women: the EPIDOS prospective study. Lancet 1996;348:511-4.
162. Durosier C, Hans D, Krieg MA, Schott AM. Prediction and discrimination of osteoporotic hip fracture in postmenopausal women. J Clin Densitom 2006;9:475-95.
163. Kanis JA, Oden A, Johnell O, Johansson H, De Laet C, Brown J, Burckhardt P, Cooper C, Christiansen C, Cummings S, Eisman JA, Fujiwara S, Gluer C, Goltzman D, Hans D, Krieg MA, La Croix A, McCloskey E, Mellstrom D, Melton LJ 3rd, Pols H, Reeve J, Sanders K, Schott AM, Silman A, Torgerson D, van Staa T, Watts NB, Yoshimura N. The use of clinical risk factors enhances the performance of BMD in the prediction of hip and osteoporotic fractures in men and women. Osteoporos Int 2007;18:1033-46.
164. Bazzocchi A, Filonzi G, Ponti F, Albisinni U, Guglielmi G, Battista G. Ultrasound: Which role in body composition? Eur J Radiol 2016;85:1469-80.
165. Pillen S, van Alfen N. Skeletal muscle ultrasound. Neurol Res 2011;33:1016-24.
166. Takai Y, Ohta M, Akagi R, Kato E, Wakahara T, Kawakami Y, Fukunaga T, Kanehisa H. Applicability of ultrasound muscle thickness measurements for predicting fat-free mass in elderly population. J Nutr Health Aging 2014;18:579-85.
167. Berger J, Bunout D, Barrera G, de la Maza MP, Henriquez S, Leiva L, Hirsch S. Rectus femoris (RF) ultrasound for the assessment of muscle mass in older people. Arch Gerontol Geriatr 2015;61:33-8.
168. Seymour JM, Ward K, Sidhu PS, Puthucheary Z, Steier J, Jolley CJ, Rafferty G, Polkey MI, Moxham J. Ultrasound measurement of rectus femoris cross-sectional area and the relationship with quadriceps strength in COPD. Thorax 2009;64:418-23.
169. Reeves ND, Maganaris CN, Narici MV. Ultrasonographic assessment of human skeletal muscle size. Eur J Appl Physiol 2004;91:116-8.
170. Sanada K, Kearns CF, Midorikawa T, Abe T. Prediction and validation of total and regional skeletal muscle mass by ultrasound in Japanese adults. Eur J Appl Physiol 2006;96:24-31.
171. Narici M, Franchi M, Maganaris C. Muscle structural assembly and functional consequences. J Exp Biol 2016;219:276-84.
172. Minetto MA, Caresio C, Menapace T, Hajdarevic A, Marchini A, Molinari F, Maffiuletti NA. Ultrasound-Based Detection of Low Muscle Mass for Diagnosis of Sarcopenia in Older Adults. PM R 2016;8:453-62.
173. Guglielmi G, Diano D, Ponti F, Bazzocchi A. Quality Assurance in Bone Densitometry. Curr Radiol Rep 2013;2:33.
174. Guglielmi G, Damilakis J, Solomou G, Bazzocchi A. Quality assurance of imaging techniques used in the clinical management of osteoporosis. Radiol Med 2012;117:1347-54.
175. Ihalainen TM, Lonnroth NT, Peltonen JI, Uusi-Simola JK, Timonen MH, Kuusela LJ, Savolainen SE, Sipila OE. MRI quality assurance using the ACR phantom in a multi-unit imaging center. Acta Oncol 2011;50:966-72.
176. Kim HS, Yang SO. Quality Control of DXA System and Precision Test of Radio-technologists. J Bone Metab 2014;21:2-7.
177. Elliot JR, Fenton AJ, Young T, Mansfield A, Burton C, Wilkinson TJ. The precision of digital X-ray radiogrammetry compared with DXA in subjects with normal bone density or osteoporosis. J Clin Densitom 2005;8:187-90.
178. Jorgensen JT, Andersen PB, Rosholm A, Bjarnason NH. Digital X-ray radiogrammetry: a new appendicular bone densitometric method with high precision. Clin Physiol 2000;20:330-5.

 

179. Hoff M, Dhainaut A, Kvien TK, Forslind K, Kalvesten J, Haugeberg G. Short-time in vitro and in vivo precision of direct digital X-ray radiogrammetry. J Clin Densitom 2009;12:17-21.
180. Lang TF. Quantitative computed tomography. Radiol Clin North Am 2010;48:589-600.
181. MacNeil JA, Boyd SK. Improved reproducibility of high-resolution peripheral quantitative computed tomography for measurement of bone quality. Med Eng Phys 2008;30:792-9.
182. Baim S, Wilson CR, Lewiecki EM, Luckey MM, Downs RW Jr, Lentle BC. Precision assessment and radiation safety for dual-energy X-ray absorptiometry: position paper of the International Society for Clinical Densitometry. J Clin Densitom 2005;8:371-8.
183. Baim S, Binkley N, Bilezikian JP, Kendler DL, Hans DB, Lewiecki EM, Silverman S. Official Positions of the International Society for Clinical Densitometry and executive summary of the 2007 ISCD Position Development Conference. J Clin Densitom 2008;11:75-91.
184. Swinford RR, Warden SJ. Factors affecting short-term precision of musculoskeletal measures using peripheral quantitative computed tomography (pQCT). Osteoporos Int 2010;21:1863-70.
185. Thijssen JM, Weijers G, de Korte CL. Objective performance testing and quality assurance of medical ultrasound equipment. Ultrasound Med Biol 2007;33:460-71.
186. Paggiosi MA, Blumsohn A, Barkmann R, Eastell R. Effect of temperature on the longitudinal variability of quantitative ultrasound variables. J Clin Densitom 2005;8:436-44.
187. Krieg MA, Cornuz J, Hartl F, Kraenzlin M, Tyndall A, Hauselmann HJ, Lippuner K, Rizzoli R, Buche D, Theiler R, Dambacher MA, Neff M, Pancaldi P, Tanzi F, Wimpfheimer K, Burckhardt P. Quality controls for two heel bone ultrasounds used in the Swiss Evaluation of the Methods of Measurement of Osteoporotic Fracture Risk Study. J Clin Densitom 2002;5:335-41.
188. Strasser EM, Draskovits T, Praschak M, Quittan M, Graf A. Association between ultrasound measurements of muscle thickness, pennation angle, echogenicity and skeletal muscle strength in the elderly. Age 2013;35:2377-88.
189. Lerski RA, de Certaines JD. Performance assessment and quality control in MRI by Eurospin test objects and protocols. Magn Reson Imaging 1993;11:817-33.
190. De Wilde J, Price D, Curran J, Williams J, Kitney R. Standardization of performance evaluation in MRI: 13 Years' experience of intersystem comparison. Concepts Magn Reson 2002;15:111-6.
191. Price RR, Axel L, Morgan T, Newman R, Perman W, Schneiders N, Selikson M, Wood M, Thomas SR. Quality assurance methods and phantoms for magnetic resonance imaging: report of AAPM nuclear magnetic resonance Task Group No. 1. Med Phys 1990;17:287-95.
192. Chen CC, Wan YL, Wai YY, Liu HL. Quality assurance of clinical MRI scanners using ACR MRI phantom: preliminary results. J Digit Imaging 2004;17:279-84.
193. Weinreb J, Wilcox PA, Hayden J, Lewis R, Froelich J. ACR MRI accreditation: yesterday, today, and tomorrow. J Am Coll Radiol 2005;2:494-503.
194. Cauley JA, Hochberg MC, Lui LY, Palermo L, Ensrud KE, Hillier TA, Nevitt MC, Cummings SR. Long-term risk of incident vertebral fractures. JAMA 2007;298:2761-7.
195. Bazzocchi A, Fuzzi F, Garzillo G, Diano D, Rimondi E, Merlino B, Moio A, Albisinni U, Battista G, Guglielmi G. Reliability and accuracy of scout CT in the detection of vertebral fractures. Br J Radiol 2013;86:20130373.
196. Bazzocchi A, Spinnato P, Garzillo G, Ciccarese F, Albisinni U, Mignani S, Battista G, Rossi C. Detection of incidental vertebral fractures in breast imaging: the potential role of MR localisers. Eur Radiol 2012;22:2617-23.
197. Klotzbuecher CM, Ross PD, Landsman PB, Abbott TA 3rd, Berger M. Patients with prior fractures have an increased risk of future fractures: a summary of the literature and statistical synthesis. J Bone Miner Res 2000;15:721-39.
198. Bazzocchi A, Guglielmi G. Vertebral Fracture Identification. Semin Musculoskelet Radiol 2016;20:317-29.
199. Bazzocchi A, Spinnato P, Fuzzi F, Diano D, Morselli-Labate AM, Sassi C, Salizzoni E, Battista G, Guglielmi G. Vertebral fracture assessment by new dual-energy X-ray absorptiometry. Bone 2012;50:836-41.
200. Bazzocchi A, Diano D, Battista G, Albisinni U, Rossi C, Guglielmi G. New dual-energy X-ray absorptiometry equipment in the assessment of vertebral fractures: technical limits and software accuracy. Skeletal Radiol 2012;41:823-9.
201. Guglielmi G, Diacinti D, van Kuijk C, Aparisi F, Krestan C, Adams JE, Link TM. Vertebral morphometry: current methods and recent advances. Eur Radiol 2008;18:1484-96.
202. Diacinti D, Guglielmi G. Vertebral morphometry. Radiol Clin North Am 2010;48:561-75.
203. Chou SH, Vokes T. Vertebral Morphometry. J Clin Densitom 2016;19:48-53.
204. Wáng YX, Santiago FR, Deng M, Nogueira-Barbosa MH.

 

Identifying osteoporotic vertebral endplate and cortex fractures. Quant Imaging Med Surg 2017;7:555-91.
205. Schwartz EN, Steinberg D. Detection of vertebral fractures. Curr Osteoporos Rep 2005;3:126-35.
206. Genant HK, Wu CY, van Kuijk C, Nevitt MC. Vertebral fracture assessment using a semiquantitative technique. J Bone Miner Res 1993;8:1137-48.
207. Vokes T, Bachman D, Baim S, Binkley N, Broy S, Ferrar L, Lewiecki EM, Richmond B, Schousboe J. Vertebral fracture assessment: the 2005 ISCD Official Positions. J Clin Densitom 2006;9:37-46.
208. Grigoryan M, Guermazi A, Roemer FW, Delmas PD, Genant HK. Recognizing and reporting osteoporotic vertebral fractures. Eur Spine J 2003;12 Suppl 2:S104-12.
209. Kanis JA, Burlet N, Cooper C, Delmas PD, Reginster JY, Borgstrom F, Rizzoli R. European guidance for the diagnosis and management of osteoporosis in postmenopausal women. Osteoporos Int 2008;19:399-428.
210. Griffith JF. Identifying osteoporotic vertebral fracture. Quant Imaging Med Surg 2015;5:592-602.
211. Jiang G, Eastell R, Barrington NA, Ferrar L. Comparison of methods for the visual identification of prevalent vertebral fracture in osteoporosis. Osteoporos Int 2004;15:887-96.
212. Ensrud KE. Epidemiology of fracture risk with advancing age. J Gerontol A Biol Sci Med Sci 2013;68:1236-42.
213. Bazzocchi A, Garzillo G, Fuzzi F, Diano D, Albisinni U, Salizzoni E, Battista G, Guglielmi G. Localizer sequences of magnetic resonance imaging accurately identify osteoporotic vertebral fractures. Bone 2014;61:158-63.
214. Adams JE. Opportunistic Identification of Vertebral Fractures. J Clin Densitom 2016;19:54-62.
215. Woo EK, Mansoubi H, Alyas F. Incidental vertebral fractures on multidetector CT images of the chest: prevalence and recognition. Clin Radiol 2008;63:160-4.
216. Smith-Bindman R, Miglioretti DL, Johnson E, Lee C, Feigelson HS, Flynn M, Greenlee RT, Kruger RL, Hornbrook MC, Roblin D, Solberg LI, Vanneman N, Weinmann S, Williams AE. Use of diagnostic imaging studies and associated radiation exposure for patients enrolled in large integrated health care systems, 1996-2010. JAMA 2012;307:2400-9.
217. Samelson EJ, Christiansen BA, Demissie S, Broe KE, Zhou Y, Meng CA, Yu W, Cheng X, O'Donnell CJ, Hoffmann U, Genant HK, Kiel DP, Bouxsein ML. Reliability of vertebral fracture assessment using multidetector CT lateral scout views: the Framingham Osteoporosis Study. Osteoporos Int 2011;22:1123-31.
218. Kim YM, Demissie S, Eisenberg R, Samelson EJ, Kiel DP, Bouxsein ML. Intra-and inter-reader reliability of semi-automated quantitative morphometry measurements and vertebral fracture assessment using lateral scout views from computed tomography. Osteoporos Int 2011;22:2677-88.
219. Griffith JF, Guglielmi G. Vertebral fracture. Radiol Clin North Am 2010;48:519-29.

**Cite this article as:** Guerri S, Mercatelli D, Aparisi Gómez MP, Napoli A, Battista G, Guglielmi G, Bazzocchi A. Quantitative imaging techniques for the assessment of osteoporosis and sarcopenia. Quant Imaging Med Surg 2018;8(1):60-85. doi: 10.21037/qims.2018.01.05

 